



HAL
open science

The Catalan magnetic anomaly: Its significance for the crustal structure of the Gulf of Lion passive margin and relationship to the Catalan transfer zone

Albane Canva, Isabelle Thinon, Aurélie Peyrefitte, Renaud Couëffé, Agnès Maillard, Laurent Jolivet, Guillaume Martelet, Frédéric Lacquement, Pol Guennoc

► To cite this version:

Albane Canva, Isabelle Thinon, Aurélie Peyrefitte, Renaud Couëffé, Agnès Maillard, et al.. The Catalan magnetic anomaly: Its significance for the crustal structure of the Gulf of Lion passive margin and relationship to the Catalan transfer zone. *Marine and Petroleum Geology*, 2020, 113, pp.104174. <10.1016/j.marpetgeo.2019.104174>. <hal-03488689>

HAL Id: hal-03488689

<https://hal.science/hal-03488689v1>

Submitted on 21 Jul 2022

HAL is a multi-disciplinary open access archive for the deposit and dissemination of scientific research documents, whether they are published or not. The documents may come from teaching and research institutions in France or abroad, or from public or private research centers.

L'archive ouverte pluridisciplinaire HAL, est destinée au dépôt et à la diffusion de documents scientifiques de niveau recherche, publiés ou non, émanant des établissements d'enseignement et de recherche français ou étrangers, des laboratoires publics ou privés.



Distributed under a Creative Commons CC BY-NC 4.0 - Attribution - Non-commercial use - International License

1 The Catalan magnetic anomaly: Its significance for the crustal structure of the Gulf of Lion
2 passive margin and relationship to the Catalan transfer zone

3

4 **Albane Canva^{a*}, Isabelle Thinon^{a*}, Aurélie Peyrefitte^{a*}, Renaud Couëffé^a, Agnès**
5 **Maillard^b, Laurent Jolivet^c, Guillaume Martelet^a, Frédéric Lacquement^a, Pol Guennoc^a**

6

7 ^aBRGM, GeoResources Division, 3 avenue Claude Guillemin, 45 060 Orleans, France

8 ^bGET, UMR 5563, Observatoire Midi-Pyrénées, 14 avenue Edouard Belin, 31400 Toulouse,
9 France

10 ^cISTEP, Sorbonne Université, Rue de l'école de Médecine, 75 006 Paris, France

11

12 * Corresponding author.

13 Fax: + 33 2 38 64 33 33.

14 E-mail address: albanecanva@msn.com (A. Canva); a.peyrefitte@brgm.fr (A. Peyrefitte);
15 i.thinon@brgm.fr (I. Thinon).

16 BRGM, DGR/GBS, 3 avenue Claude Guillemin, 45 100 Orléans, France

17

18

19

20
21 **ABSTRACT**

22 The western part of the Gulf of Lion (GoL) passive margin, at the foot of the Pyrenees mountain
23 chain hosts the Catalan magnetic anomaly (CMA), a significant NW-SE-trending linear magnetic
24 anomaly 50 km long with no associated gravimetric signal. The CMA is located on the continental
25 slope near the NW-SE-trending Catalan transfer zone (CTZ), and it extends from the shelfbreak to the
26 abyssal plain across thinned to hyper-thinned continental domain. This study interprets an updated
27 geophysical dataset to better understand the Pyrenees–GoL transition and proposes a new
28 interpretation of the CMA’s source. Gravimetric and magnetic modelling of the lithosphere along two
29 perpendicular cross-sections indicates that the CMA is generated by a magnetic body ($80 \times 20 \times 12$
30 km) , called here the Catalan body within the thinned continental domain. We interpret it as a mass of
31 mafic material underplating and intruding the continental crust along a crustal fault belonging to the
32 CTZ system. From the new map of Moho depths, a wide NW-SE-trending zone is highlighted on the
33 western extremity of the GoL margin at the foot of the eastern Pyrenees Chain. It is characterized by
34 (i) a heterogeneous crustal structure and mantle rise underneath the Tertiary Catalan sedimentary basin
35 in the continental shelf area, (ii) a necking zone in a more proximal location compared to the eastern
36 GoL margin, and (iii) the presence of the magmatism (Catalan body) under and in the thinned
37 continental crust, in the necking zone domain. These characteristics may be induced by the
38 transtensional motion along the CTZ during the Tertiary opening of the Liguro-Provençal Basin,
39 contemporary with the extension of the GoL margin. However, the role of inherited structures from
40 the Hercynian orogeny, Mesozoic rifting and Pyrenean orogeny cannot be excluded when explaining
41 the crustal heterogeneity, transfer zones and Moho morphology in this region.

42

43 ***Keywords:***

44 Gulf of Lion margin, Pyrenees, Catalan magnetic anomaly, Magnetic and gravimetric
45 modelling, Moho depth map, Transfer zone, Mafic magmatic intrusion, Underplating

46

47 **1. Introduction**

48 The formation of mountain ranges and subsequent postorogenic thinning are major topics of
49 debate. In the western Mediterranean, the Pyrenean orogenic belt ends abruptly at the Gulf of Lion
50 (GoL) passive margin, and after decades of work in this area, explaining this termination of the eastern
51 Pyrenees remains a challenge.

52 Between the Pyrenees and the GoL margin (**Fig. 1**), a major transfer zone called the Catalan
53 transfer zone (CTZ; [Mauffret *et al.*, 2001](#)) is widely considered to have played a major role in the
54 opening of the GoL and the Liguro-Provençal Basin. The position of the CTZ also coincides with the
55 edge of a major magnetic anomaly (**Fig. 1**). Since 1965, when comprehensive aeromagnetic data were
56 first acquired in this region, published hypotheses have not resulted in realistic interpretations of this
57 anomaly, which is a key feature of the GoL margin.

58 Magnetic anomalies are relatively common features of rift systems, such as the East Africa rift
59 (e.g. [Buck, 2006](#)), the Aden-Afar rift (e.g. [Bridges *et al.*, 2012](#)) and the Red Sea rift (e.g. [Ligi *et al.*,
60 2018](#)). They also are common on volcanic continental margins, such as the Vøring and Namibia
61 margins (e.g. [White *et al.*, 1987](#); [Geoffroy, 2005](#); [Bauer *et al.*, 2000](#)), and are known in nonvolcanic
62 margins as well. These magnetic anomalies have been interpreted variously as indicating the presence
63 of mafic intrusions in the exhumed or hyperextended continental crust (Northern Red Sea margin, [Ligi
64 *et al.*, 2018](#); Galicia passive margin, [Schärer *et al.*, 1995](#); Iberian margin, [Neres *et al.*, 2018](#)), mafic
65 underplating coupled with basaltic intrusions (Newfoundland-Iberia rift system, [Bronner *et al.*, 2011](#);
66 [Thybo & Artemieva, 2013](#)), or strongly serpentinized mantle (e.g. [Dunlop & Prévot, 1982](#); [Shive *et*
67 *al.*, 1988](#); [Sibuet *et al.*, 2007](#)). In the Liguro-Provençal Basin and Valencia Trough, volcanic edifices
68 have been shown to be related to subduction slab retreat (e.g. [Maillard & Mauffret, 1999](#); [Séranne,
69 1999](#); [Jolivet & Faccenna, 2000](#); [Jolivet *et al.*, 2006](#); [Réhault *et al.*, 2012](#); **Fig. 1** and **Fig. 2**). Some of
70 those volcanic bodies also coincide with strong magnetic anomalies ([Maillard & Mauffret, 1993](#);
71 [Rollet *et al.*, 2002](#)).

72 The significant NW-SE-trending magnetic anomaly in the southwestern GoL (**Fig. 1**) is called
73 hereafter the Catalan magnetic anomaly (CMA), due to its location off the coast of the Catalan region.

74 A smaller but almost as intense magnetic anomaly to the east of the CMA is called anomaly B
75 hereafter

76 In this paper, we interpret both magnetic anomalies, with a special focus on the CMA, using
77 magnetic and gravimetric modelling along two cross-sections (M1 and M2 in **Fig. 2**). We propose a
78 consistent geological interpretation of these anomalies in terms of crustal geometry and an explanation
79 of the role of the structures associated with them in the transition between the Pyrenees and the GoL.

80

81 **2. Geological setting**

82 The GoL margin (**Fig. 2**) is a segment of the northern continental margin of the Liguro-
83 Provençal oceanic basin, which is interpreted as a back-arc basin that formed as a result of the 30°
84 anticlockwise rotation of the Corsica-Sardinia block during the retreating phase of Apennine
85 subduction (e.g. [Réhault *et al.*, 1984](#); [Gueguen *et al.*, 1998](#); [Jolivet & Faccenna, 2000](#); [Gattacceca *et al.*, 2007](#);
86 [Jolivet *et al.*, 2015](#)). The Liguro-Provençal Basin opened in two steps: a synrift stage
87 (Chattian to early Burdigalian, 30–20.5 Ma) and a postrift stage (early Burdigalian to Langhian, 20.5–
88 15 Ma) (e.g. [Gattacceca *et al.*, 2007](#)).

89 From the rifting phase into Quaternary time, volcanism has been active in the Catalan region
90 (e.g. [Bartrina *et al.*, 1992](#); [Mauffret *et al.*, 2001](#)), the Valencia Trough ([Marti *et al.*, 1992](#); [Maillard,
91 1993](#); [Maillard & Mauffret, 1993](#)) and the West Mediterranean basin. In Languedoc, long-lasting -
92 Mesozoic to Quaternary- alkaline volcanic activity trending N-S over 160 km is related to a
93 lithospheric mantle anomaly ([Liotard *et al.*, 1991](#); [Dautria *et al.*, 2010](#)). In the Corsica Liguria basins,
94 the oldest Tertiary magmatism related to the Western Mediterranean geodynamics, was mainly calc-
95 alkaline and dated at ca 35 Ma (e.g. [Réhault *et al.*, 2012](#)). Volcanic activity in the Miocene and
96 Pliocene was important on the Provence, Sardinia and Corsica margins (e.g. [Réhault *et al.*, 2012](#)).
97 These volcanic events may be an expression of hot mantle upwelling linked to the development of a
98 slab window in a postcollisional tectonic framework ([Réhault *et al.*, 2012](#); [Jolivet & Faccenna, 2000](#)).

99 During the anticlockwise rotation of the Corsica-Sardinia block, major transfer zones such as
100 the Catalan and Arlesian transfer zones appear to have played a key role in segmenting the Liguro-
101 Provençal domain into the Valencia Trough, the GoL margin and the Provençal margin (**Fig. 1** and **2**;

102 e.g. Gorini, 1993; Guennoc *et al.*, 1994, 2000; Mauffret *et al.*, 1995, 2001; Benedicto *et al.*, 1996;
103 Mauffret & Gorini, 1996; Olivet, 1996; Gueguen *et al.*, 1998; Gattacceca *et al.*, 2007; Séranne *et al.*,
104 1995; Maillard & Mauffret, 1999). These transfer zones were inferred by researchers for kinematic
105 reasons, but they are difficult to detect in observations, and no systematic study has been undertaken to
106 characterize their nature or their geometries.

107

108 **2.1. The Gulf of Lion margin**

109 The GoL continental margin extends southeast of the Cévennes fault between the Provence
110 region to the east and the Pyrenees chain and Roussillon basin to the west (**Fig. 1** and **Fig. 2**). The
111 margin is conventionally divided into five crustal domains, from the present coast to the oceanic crust,
112 on the basis of the ECORS and SARDINIA deep seismic reflection profiles (**Fig. 3**; Gorini, 1993;
113 Séranne, 1999; Gailler *et al.*, 2009; Bache *et al.*, 2010; Moulin *et al.*, 2015). The unthinned continental
114 crust domain (30 km thick) is composed of a lower and upper crust, both about 15–17 km thick. The
115 Hinge zone is the domain where the crust thins seaward from ~30 to 20 km. Further offshore, domain I
116 (**Fig. 1**, **Fig. 2** and **Fig. 3**) is about 170 km wide and consists of thinned to hyper-thinned continental
117 crust (20 km to 5 km thick) featuring horsts, grabens and tilted blocks in the upper continental crust
118 and a thinned lower continental crust (Gorini, 1993; Séranne *et al.*, 1995; Gailler *et al.*, 2009; Moulin
119 *et al.*, 2015). Its seaward edge is a slope area in which the crust thins from 20 to 7 km. On the
120 SARDINIA profile, the slope area is associated with a high-velocity body (6.5–7 km/s, **Fig. 3B**;
121 Moulin *et al.*, 2015). All along the GoL margin, domain II, a transitional domain around 100 km wide,
122 is characterized by a crust 5 km thick with anomalously high velocities (7–7.5 km/s, **Fig. 3**; Seranne,
123 1999; Moulin *et al.*, 2015). This very thin crust is interpreted as either exhumed and partially
124 serpentinized upper mantle (Boillot *et al.*, 1980, 1987, 1989; Beslier *et al.*, 1993; Guennoc *et al.*, 1994;
125 Chamot-Rooke *et al.*, 1999; Gailler *et al.*, 2009) or exhumed and thinned/stretched lower continental
126 crust (Wernicke, 1985; Séranne *et al.*, 1995; Séranne, 1999; Moulin *et al.*, 2005, 2015; Aslanian *et al.*,
127 2009; Jolivet *et al.*, 2015). Domain III consists of thin (5 km) oceanic crust (e.g. Pascal *et al.*, 1993;
128 Chamot-Rooke *et al.*, 1999; Rollet *et al.*, 2002; Gailler *et al.*, 2009).

129 In domain I on the continental shelf of the GoL margin, extensional structures predominantly
130 oriented NE-SW and their onshore counterparts overprint the Pyrenean fold-and-thrust belt. The
131 interaction of this extension tectonic features with inherited Pyrenean structures has been analysed by
132 some authors (Mauffret *et al.* 1995, 1996, 2001; Séranne *et al.*, 1995; Benedicto *et al.*, 1996). The
133 GoL shelf is divided into two distinct parts (Fig. 2). The northeastern part is characterized by a
134 succession of horsts and grabens oriented NE-SW with a thin (<2 km) cover of Cenozoic synrift and
135 postrift sedimentary formations (Guennoc *et al.*, 2000; Oudet *et al.*, 2010). The southwestern part
136 contains the wide and deep Graben Central basin, which encompasses the Catalan and Cathares basins
137 (Fig. 2). Both of these basins are filled by 6 km of Cenozoic synrift and postrift sediments (Gorini,
138 1993; Gorini *et al.*, 1994; Guennoc *et al.*, 2000; Bache *et al.*, 2010) and are separated by a transfer
139 zone (n°1 on Fig. 2) associated with a step in Moho depth from 21 to 24 km (Mauffret *et al.*, 2001).
140 The Catalan basin is underlain by a moderately thin crust and a shallow Moho (21 km from seismic
141 data in Mauffret *et al.*, 2001, Fig. 3C; 15 km from gravity modelling in Guennoc *et al.*, 1994). The
142 Moho is deeper (23–28 km) along the Catalan margin and below the so-called Rascasse horst (Fig.
143 3C). The Rascasse horst is a structure interpreted as a rollover on a deep crustal detachment (Mauffret
144 *et al.*, 2001). Several interpretations have been proposed to explain the establishment of these
145 sedimentary basins. The Catalan basin may be a Mesozoic basin, formed during Jurassic extension or
146 Cretaceous pull-apart motion, into which the Rascasse structure then slid during the Pyrenean orogeny
147 and was afterward displaced to its present position along a deep detachment during extension
148 (Mauffret *et al.*, 2001). The Graben Central basin could be related to the Liguro-Provençal back-arc
149 rifting (e.g. Réhault *et al.*, 1984; Mauffret *et al.*, 1995) or the southward Tertiary extension of the West
150 European Continental Rift system (Gorini, 1993; Séranne, 1999; Fig. 2), which ran from the Rhine
151 graben to the Valencia basin during an episode of E-W extension (Bergerat, 1987; Ziegler, 1992).
152 According to Séranne (1999), these rift basins are controlled by NE-trending extensional faults
153 overprinting the E-W-trending Pyrenean thrusts in the Provence and Languedoc regions.

154 The prerift substratum of the GoL margin is composed of Paleozoic and Mesozoic formations
155 (Fig. 2). The Palaeozoic substratum includes various lithologies (such as metasediments pelites,
156 schists, sandstones, limestones or granite) from the Variscan cycle (Guennoc *et al.*, 2000) and is

157 deformed by NE-SW-trending faults (Nîmes, Cévennes, Alès, and others) related to the late-Variscan
158 strike-slip and Tethyan rifting (e.g. [Arthaud & Matte, 1975](#); [Mascle et al., 1996](#)). Offshore, deep
159 detachments have been described in the basement beneath the Tramontane well ([Gorini et al., 1994](#))
160 and the Rascasse well ([Guennoc et al., 1994](#); [Fig. 3C](#)). In the western GoL, seismic profiles and well
161 samples show the Mesozoic sedimentary cover (sampled in Calmar or Agde Maritime 1 wells;
162 [Guennoc et al., 2000](#)) to be thin (as seen on seismic profiles), unlike the thick Mesozoic cover in the
163 Pyrenean sedimentary basins (Boucheville, Bas Agly and St. Paul de Fenouillet synclines to the north
164 of the North Pyrenean Fault and the Figueres-Montgrí basin to the south, [Fig. 2](#); e.g. [Vergés et al.,](#)
165 [2002](#); [Lagabrielle et al., 2010](#); [Tugend et al., 2014](#); [Clerc et al., 2015](#); [Chelalou et al., 2016](#); [Teixell et](#)
166 [al., 2016](#); [Wang et al., 2016](#); [Tavani et al., 2018](#)) and in the eastern GoL margin (as presumed from
167 seismic profiles; [Mauffert & Gorini, 1996](#)) and Provençal margin (Beausset syncline, [Fig. 2](#); [Bestani](#)
168 [et al., 2015](#); [Fournier et al., 2016](#)).

169 **2.2. The eastern Pyrenees**

170 The interactions between the Pyrenean thrusts and the GoL rifting are not fully understood. The
171 extent to which lithospheric heterogeneities inherited from the Hercynian and Pyrenean orogenies and
172 Mesozoic (Permian or mid-Cretaceous) rifting influenced the geometry and kinematics of the GoL
173 margin is an open question.

174 The Pyrenean belt ([Fig. 2](#) inset) is the result of the convergence between the Iberian and
175 European plates starting in the Late Cretaceous (e.g. [Choukroune et al., 1973](#); [Olivet, 1996](#)).
176 Metamorphosed Mesozoic sedimentary formations are distributed in a narrow WNW-ESE-trending
177 belt defined as the North Pyrenean Zone, bounded by two major post-metamorphic thrusts, the North
178 Pyrenean Fault (NPF) to the south and the North Pyrenean Frontal Thrust to the north. Outcrops of
179 subcontinental peridotite in the North Pyrenean Zone are attributed to mantle exhumation and crustal
180 hyperextension during the Mesozoic rift-transensional motions ([Vielzeuf & Kornprobst, 1984](#);
181 [Lagabrielle & Bodinier, 2008](#); [Clerc et al., 2015](#); [Teixell et al., 2016](#)). At a regional scale, the North
182 Pyrenean Zone is thought to represent the portion of the lithosphere that accommodated most of the
183 deformation during the anticlockwise rotation of the Iberian plate with respect to the European plate in
184 mid-Cretaceous times ([Choukroune & Mattauer, 1978](#)).

185 A recent study by [Wehr *et al.* \(2018\)](#), citing passive seismic profiles across the Pyrenees ([Diaz](#)
186 [*et al.*, 2018](#); [Chevrot *et al.*, 2018](#)), presented a 3D geometrical model of Bouguer anomalies showing a
187 Moho deeper than 50 km below the Pyrenean axial zone that is shallower (30–40 km) in the eastern
188 part (the Cap de Creus region). [Wehr *et al.* \(2018\)](#) concluded that the shallower Moho signifies a
189 missing lower crust, a possible consequence of the retreat of the Tyrrhenian slab during the opening of
190 the western Mediterranean basins. The Bouguer model also displays a shallowing of the Moho from
191 30 to 25 km in an E-W-trending area under the Roussillon basin. [Wehr *et al.* \(2018\)](#) proposed that the
192 North Pyrenean Fault extends below the Roussillon basin and accounts for this step in the Moho
193 depth. Other authors have proposed extensions of the North Pyrenean Fault into the western GoL,
194 lying north of the Catalan basin from seismic data ([Mauffret *et al.*, 2001](#)) and north of the Rascasse
195 horst from aeromagnetic data ([Guennoc *et al.*, 1994](#)). The fault is not inferred in the eastern GoL.
196 Some authors draw it at the foot of the GoL and Provençal continental margin (e.g. [Guennoc *et al.*,](#)
197 [1994](#); [Séranne, 1999](#)).

198 In the Cap de Creus region, the Variscan basement contains intrusions of diorite and other
199 granitoids (e.g. [Carreras, 2001](#); [Carreras *et al.*, 2004](#); [Druguet, 2001](#)) and NW-SE-trending shear
200 zones. Tertiary reactivation of these shear zones has been proposed at 58.57 ± 0.55 Ma ([Vissers *et al.*,](#)
201 [2016](#)) or at 69–47 Ma and 42–37 Ma ([Monié *et al.*, 2018](#); [Druguet *et al.*, 2018](#)), synchronously with
202 Pyrenean compression. The thrust sheet involving the Figueres-Montgrí basin has been dismembered
203 by a series of Neogene NW-SE-trending extensional faults associated with the North Balearic fault
204 zone (NBFZ) ([Mauffret *et al.*, 2001](#)).

205 **2.3. The Catalan transfer zone**

206 Most kinematic reconstructions imply that the rotation of the Corsica-Sardinia block involved
207 motion along a series of NW-SE transfer zones (e.g. NBFZ, CTZ, Arlesienne transfer zone; [Fig. 1](#)),
208 but these systems have never been clearly imaged and their structures are elusive ([Auzende *et al.*,](#)
209 [1973](#); [Réhault *et al.*, 1984](#); [Maillard *et al.*, 2003](#); [Granado *et al.*, 2016](#)). In particular, the abrupt
210 transition between the GoL margin and the eastern Pyrenees appears to coincide with the poorly
211 constrained CTZ ([Lefebvre, 1981](#); [Gorini *et al.*, 1993](#); [Séranne *et al.*, 1995](#); [Mauffret *et al.*, 2001](#)). The
212 CTZ runs along the Catalan margin in the Cap de Creus region ([Fig. 2](#)), where there is an abrupt

213 thickening of the crust and a dipping of the Moho toward the Pyrenees (e.g. [Nercessian et al., 2001](#);
214 [Wehr et al., 2018](#)), and below the Rascasse horst ([Mauffret et al., 2001](#)). The CTZ plays a major role
215 on tectonics and sedimentation in this area and has accommodated transtensional / extensional
216 deformation of the Rascasse horst and the coeval opening of the Catalan basin ([Mauffret et al., 1995](#),
217 [2001](#)).

218 Further south and slightly to the west, the NBTZ (e.g. [Auzende et al., 1973](#); [Rehault et al.,](#)
219 [1984](#); [Séranne, 1999](#)) (Fig. 1) separates the Valencia Trough from the deep Liguro-Provençal Basin
220 and marks the trace of the Corsica-Sardinia block during its Miocene rotation ([Fig. 2](#) inset; [Séranne,](#)
221 [1999](#); [Maillard & Mauffret, 1999](#); [Mauffret et al., 2001](#)).

222 **2.4. The Catalan magnetic anomaly**

223 The CMA appears on the magnetic map of the western Mediterranean Sea ([Galdeano &](#)
224 [Rossignol, 1977](#)) as a strong linear magnetic anomaly ([Fig. 1](#)). Seismic reflection profiles ([Gorini et](#)
225 [al., 1993](#); [Guennoc et al., 1994](#); [Mauffret et al., 2001](#)) show no evidence of volcanic intrusions in the
226 postrift and synrift sedimentary cover in the CMA area (Catalan basin and Rascasse horst; [Fig. 2](#)).

227 From gravity modelling, [Guennoc et al. \(1994\)](#) interpreted a possible mantle rise under the
228 Catalan basin that is in accordance with [Mauffret et al. \(2001\)](#). According to [Guennoc et al. \(1994\)](#),
229 the CMA represents a body with strong magnetization, induced either by shallow intrusions (6–10 km)
230 or by the combination of a shallow Moho (17–15 km) and intrusions at depths between 11 and 14 km.
231 Those intrusions would be located under the shallow detachment observed by [Mauffret &](#)
232 [Gennesseaux \(1989\)](#) and [Mauffret et al. \(2001\)](#), in the Palaeozoic basement under the Rascasse horst,
233 because the reflector associated to this structure is continuous ([Fig. 3C](#)). These authors suggested, by
234 analogy with gravity anomalies along the Pyrenean belt and Mediterranean margins, that the intrusions
235 resulted from two phases of magmatic intrusions into the continental crust. Intrusions of the first phase
236 (Triassic or Early Cretaceous) occurred at depth, near the base of the continental crust. Indeed,
237 Triassic and Cretaceous intrusions in the Pyrenees have similar magnetic susceptibility values
238 ([Azambre & Pozzi, 1982](#)). Intrusions of the second phase occurred during Cenozoic extension,
239 consistent with transtensional motions along major NW-SE-trending structures (CTZ and NBTZ), as a
240 leaky transform described in the North Balearic Islands ([Mauffret et al., 1992](#)).

241

242 **3. Geophysical data, processing and mapping**

243 For this study, we compiled gravimetric and magnetic data covering most of the GoL area and
244 we then established a complete Bouguer anomaly map (**Fig. 4**) and a reduced-to-the-pole (RTP)
245 magnetic anomaly map (**Fig. 5**), respectively. To constrain the geophysical models, we used some
246 available interpreted seismic sections across the GoL margin and also took into account the geological
247 formations outcropping along the coastline and those sampled by oil exploration wells offshore.

248 **3.1. Gravimetric data and the Bouguer anomaly map**

249 The gravimetric data compilation includes offshore and onshore data. For the offshore domain,
250 Compagnie Générale de Géophysique (CGG) seafloor gravity data (1966), data from several marine
251 campaigns archived at IFREMER-SISMER, and an Elf-Explo campaign of 1996 allowed us to cover
252 the entire GoL margin. The onshore domain was covered by ground surveys archived in the Banque
253 Gravimétrique de la France ([Martelet et al., 2009](#)) for French territory and in the International
254 Gravimetric Bureau database (<http://bgi.obs-mip.fr/>) for Spain.

255 The combined gravity dataset was carefully reprocessed to align all data with the IGSN71–
256 Hayford 1930 gravity reference system. State-of-the-art gravity data reduction was performed,
257 including free-air and Bouguer slab reduction in which a Bouguer reference density of 2.3 g/cm^3 was
258 used, considering that most data points are located above sedimentary basins. Terrain corrections were
259 computed using a procedure after [Martelet et al. \(2002\)](#). Topographic and bathymetric datasets used
260 for free air and Bouguer corrections were made using the IGN digital terrain model topographic
261 dataset (250 m resolution) onshore and the EMODnet bathymetric grid (200 m resolution) offshore
262 (<http://www.emodnet-bathymetry.eu>). Terrain corrections were computed from 200 m to 10 km
263 around the gravity stations, using topographic grids resampled every 200 m, and from 10 km to 167
264 km using topographic grids resampled every 1 km.

265 Offshore gravity data were reduced, first by trimming the data from different marine campaigns
266 in order to reduce navigation noise and homogenize data sampling. Instrumental drift was reduced
267 using traditional adjustments at profile intersections, first for each survey and then between different
268 surveys, considering the Elf Explo 1996 cruise as the reference. The CGG 1966 seafloor gravity data

269 was upward-continued to the sea surface before being merged with other datasets. The resulting
270 dataset was finally converted to a 1-km regular grid using a minimum curvature algorithm.

271 The complete Bouguer anomaly map (**Fig. 4**) incorporates all the density contrasts below the
272 topography. Anomalies range from -264 to $+194$ mGal and display a regional gravity gradient in
273 which anomalies are mostly negative onshore and positive offshore, highlighting the land-sea
274 transition. At first glance, some gravity anomalies appear to correspond to major geological structures,
275 such as the Nîmes fault.

276 **3.2. Magnetic data and the magnetic anomaly map**

277 The airborne magnetic dataset was acquired in 1965 by CGG using a CSF magnetometer and a
278 Toran positioning system flown at a constant altitude of 900 m above sea level. Magnetic data were
279 collected along flight lines spaced 3 km apart in the NW-SE direction and 12 km apart in the
280 perpendicular direction. After reduction of diurnal variations of the magnetic field, data were
281 interpolated on a 1000-m regular grid using bidirectional gridding. The operator originally applied a
282 regional correction of $+2.8$ nT/km along the SE-NW flight lines and -0.3 nT/km along the SW-NE
283 lines. We back-corrected this regional trend and adopted a standard regional magnetic reduction based
284 on the International Geomagnetic Reference Field (IGRF) for the date of the survey. Next, a state-of-
285 the-art reduction to the pole (RTP) filter was applied to the dataset, relocating the anomalies directly
286 above their sources, to improve the interpretation of magnetic source locations relative to geologic
287 features. The resulting RTP magnetic anomaly map (**Fig. 5**) displays geomagnetic field strengths
288 ranging from 2950 to 3200 nT. Despite the removal of the long-wavelength IGRF, a SW-NE gradient
289 is apparent. Various rather large magnetic anomalies are observed along the coast line and onshore in
290 figure 5. These seem related to onshore tectonics/structures as the Pyrenean belt or the Nîmes fault for
291 example. The largest magnetic anomaly observed is the CMA. Because of its amplitude, trend and
292 location, and because we cannot associate it to known tectonics features, unlike the other anomalies,
293 we decided to aim our study to understand the CMA and the anomaly B.

294

295 **4. 2D geophysical modelling**

296 Gravimetric and magnetic modelling consists of simulating the distributions of density and
297 magnetic susceptibility that best explain the measured geophysical data. In practice, after positioning
298 the geophysical profiles to be modelled, a 2D geological model is created. Each layer of this model is
299 assigned values of density and magnetic susceptibility to allow the computation of modelled
300 gravimetric and magnetic effects. Displaying the measured Bouguer anomaly and RTP magnetic
301 anomaly data along specific profiles allows a direct visual comparison of observed and modelled
302 geophysical effects.

303 Many models were tested by modifying the geometry of the starting model to best match the
304 geophysical responses of the model with the observed geophysical data. Different structures and
305 bodies can equally well explain the measured signal. Therefore, it is necessary to introduce as many
306 structural constraints and as much field information as possible during the modelling process to reduce
307 the inherent uncertainty of the method. In this process, knowledge of the geological context is
308 important to test the most meaningful hypotheses. The shape, wavelength and intensity of gravimetric
309 and magnetic anomalies allow to address the size, intensity and depth of density contrasts. In our
310 investigation of the CMA and anomaly B, we modelled two perpendicular cross-sections, M1 and M2
311 (**Fig. 2** and **Fig. 5**).

312 Cross-section M1 oriented NW-SE, crosses the whole GoL margin from the inner continental
313 shelf to the abyssal plain. From the unthinned continental domain to the oceanic domain, it goes along
314 the CMA's axis of higher amplitude and goes through the Catalan basin. This cross-section is parallel
315 and close to (~15 km east) the SARDINIA seismic profile, which doesn't cross the higher values of
316 the CMA (lower values at the end of extension).

317 Cross-section M2 oriented SW-NE, intersects the CMA, anomaly B and the SARDINIA and
318 ECORS seismic profiles. It runs from Cap de Creus (Pyrenean crust) to Marseille (Provençal crust),
319 along the present shelf break.

320 **4.1. The 2D geometric model**

321 Our geophysical cross-sections were computed from a 2D geometric model containing multiple
322 layers, each characterized by specific densities and magnetic susceptibilities. Remanent magnetization

323 was not considered because no strong remanent anomalies appear in the RTP map (Fig. 5). The layer-
324 cake model (Fig. 6) extends through the lithosphere to 50 km depth and extends laterally to infinity in
325 order to avoid edge effects. Because our model integrates deep density contrasts down to the Moho,
326 the complete Bouguer anomaly is used rather than a residual Bouguer anomaly more appropriate for
327 relatively superficial layers. Our initial model is defined by the following five layers:

- 328 • The water layer is defined by zero elevation (top) and the EMODnet bathymetry grid (base).
- 329 • The Tertiary sedimentary cover encompasses synrift and postrift formations, with mainly
330 detrital lithologies (Gorini *et al.*, 1993; Guennoc *et al.*, 2000). The base of this cover is derived
331 from interpreted seismic data (Couëffe *et al.*, 2016). This layer includes three sublayers that
332 gradually increase in density with depth in order to take into account diagenetic effects. From
333 top to bottom, the density values are 2350 kg/m³, 2400 kg/m³ and 2600 kg/m³ based on the
334 gravimetric cross-sections of Guennoc *et al.* (1994) and common values from Berndt *et al.*
335 (2001) and Keen *et al.* (2018).
- 336 • The upper continental crust is delimited on the basis of the SARDINIA seismic velocity model
337 (Moulin *et al.*, 2015; Fig. 3A), and its density (2750 kg/m³) is adapted from the three-layered
338 global model CRUST1.0 (Laske *et al.*, 2012). For 2D modelling, the Paleozoic and Mesozoic
339 prerift formations are integrated in this layer because their density (2700 kg/m³, Guennoc *et*
340 *al.*, 1994) is similar, their thickness is negligible in the CMA area and their extent is not well
341 mapped.
- 342 • The lower continental crust is based on the interpreted ECORS seismic profile (Séranne, 1999;
343 Fig. 3B) and the seismic interface of Diaz *et al.* (2018). Its density, also adapted from
344 CRUST1.0, is set at 2950 kg/m³.
- 345 • The lithospheric mantle is defined by the Moho geometry, compiled from many authors (e.g.
346 Chamot-Rooke *et al.*, 1999; Gallart *et al.*, 2001; Mauffret *et al.*, 2001; Nercessian *et al.*, 2001;
347 Gailler *et al.*, 2009; Diaz *et al.*, 2018; Wehr *et al.*, 2018) and from CRUST1.0 in otherwise
348 unconstrained areas. Its density of 3360 kg/m³ is a conventional value for the average upper
349 mantle (Braun & Beaumont, 1989).

350 The boundaries between the continental (I), transitional (II) and oceanic (III) domains are
351 derived from the interpreted seismic profiles (Séranne, 1999; Gailler *et al.*, 2009; Bache *et al.*, 2010;
352 Moulin *et al.*, 2015). The transitional (II) and oceanic (III) domains are outside the area where high-
353 resolution data from the 1965 aeromagnetic survey are available, thus no hypothesis concerning their
354 crustal magnetization could be tested. Therefore, we set their magnetic susceptibility to null as it did
355 not affect the calculated magnetic signal. The crust of the transitional domain is characterized by a
356 velocity between those of the lower crust and mantle (Moulin *et al.*, 2015), and accordingly its density
357 should be in between mantle and lower crust densities. We applied a density of 2850 kg/m³
358 (comparable to Elo, 1997) for the oceanic crust of domain III.

359 The sedimentary cover, upper and lower continental crusts and the mantle are considered to be
360 nonmagnetic in our models. Crustal geometry and domain limits provided by the SARDINIA and
361 ECORS seismic profiles (Fig. 3) and the geological formations outcropping along the coastline and
362 sampled by offshore wells (Fig. 2) were also taken into account.

363 Note that in the following, the geometries of the water layer (bathymetry values, Fig. 2) and the
364 sedimentary cover (Fig. 2, 3; Gorini 1993; Guennoc *et al.*, 2000; Bache *et al.*, 2010; Coueffé *et al.*,
365 2016) were not modified as they are closely constrained by data whereas the other limits were adjusted
366 to best fit the data.

367 **4.2. Geological hypotheses**

368 Considering the lobate shape of the CMA, the corresponding magnetized body must consist of
369 two separate parts to coincide with the structure suggested by the magnetic data (Fig. 5). Considering
370 the strong intensity of the CMA, the magnetic body must either be very thick or have an extremely
371 high magnetic susceptibility. Because of the long wavelength of this anomaly, modelling shows that
372 the source body must be deeper than 5 km, thus below the sedimentary cover. The absence of any
373 gravimetric feature over the CMA (Fig. 4) attests that the magnetized body must have a density close
374 to its surroundings.

375 To reduce the range of possible models for the CMA, we tested seven geological hypotheses
376 (H1 through H7 in Table 1) consistent with the geologic and geodynamic context seen in other

377 continental margins with magnetic anomalies. These involved four basic sources for the geophysical
378 signal of the CMA:

- 379 • A basaltic body (H1 and H3). Basaltic intrusions have been described as volcanic seamounts
380 at the top of the substratum in surrounding areas (Valencia Trough from [Maillard, 1993](#) and
381 [Mauffret et al., 1995](#); Corsica margin from [Réhault et al., 2012](#)).
- 382 • A gabbroic body (H4 and H5). Gabbroic intrusions, mafic contamination and mafic
383 underplating have been described on the Vöring volcanic continental margin ([Berndt et al.,](#)
384 [2001](#)) and the Iberia nonvolcanic continental margin ([Neres et al., 2018](#)), and gabbroic sills
385 and dykes have been described in the upper continental crust of other margins (e.g. Northern
386 Red Sea margin; [Ligi et al., 2018](#)).
- 387 • A mix of basalt and gabbro bodies (H2), as described in the Newfoundland-Iberia conjugate
388 rift system ([Bronner et al., 2011](#)).
- 389 • A body of serpentinized mantle (H6 and H7), as described in the central Labrador margin
390 ([Keen et al., 2018](#)).

391 Due to the size and intensity of the CMA, magnetic susceptibilities were initially based on
392 published studies and then modified during modelling. For each hypothesis, the density was fixed,
393 whereas the shape and magnetic susceptibility of the modelled body were adjusted over several
394 iterations, taking into account the geological possibilities, to properly fit the model to the observed
395 geophysical data along the two cross-sections.

396

397 **5. Modelling results and key observations**

398 The CMA is 50 km long and 20 km wide. It has a magnetic amplitude as great as 3450 nT ([Fig.](#)
399 [5](#)). This anomaly lies entirely within domain I, which is characterized by thinned continental crust
400 under the continental slope ([Fig. 2](#)). The observed magnetic and gravimetric signals along cross-
401 sections M1 and M2 are shown in [Fig. 7](#).

402 ***5.1. Selection of working hypotheses best fitting the geophysical signal***

403 For each proposed hypothesis, the intensity and shape of the calculated magnetic signal could be
404 adjusted to match the observed magnetic signal, except for H1, which could not quite be made to fit

405 the curve. Concerning the gravimetric data, the resulting magnetic bodies led to a mass excess for H1
406 to H4 and a mass deficit for H6 and H7 (**Table 1**).

407 The presence of a high-velocity body in the thinned continental domain on the SARDINIA
408 seismic profile (domain I, **Fig. 3**) favours the three hypotheses that include a dense body beneath the
409 thinned continental crust (H2, H4 and H5, **Table 1**).

410 We ruled out H1 and H2 because neither volcanic seamounts nor sills/dykes have been
411 described in the seismic profiles or sampled in the area of the CMA (Rascasse well; *Gorini et al.*,
412 1993; *Mauffret et al.*, 1995; *Guennoc et al.*, 2000). Moreover, the continuity of the detachments in the
413 Paleozoic basement there weighs against the presence of magmatic bodies above (*Guennoc et al.*,
414 1994).

415 Hypotheses H6 and H7, involving a body of serpentinized mantle, were carefully tested. But the
416 degree of serpentinization must be quite high to obtain the intensity of the CMA. *Maffione et al.*
417 (2014) measured magnetic susceptibility values greater than 0.02 SI for a degree of serpentinization
418 higher than 60%, which would imply a density lower than 2540 kg/m³ (*Miller & Christensen*, 1997).
419 The shape of the CMA's magnetic signal thus could be explained only by a high degree of
420 serpentinization over a large volume, which is inconsistent with the geological context, leading us to
421 dismiss H6 and H7. Moreover, those hypotheses led to a mass deficit inconsistent with the gravimetric
422 signal (**Table 1**).

423 After many different tests, the most successful hypothesis was H5, which implies the occurrence
424 of mafic rocks of gabbroic type at depth (**Table 1** and **Fig. 7**). These igneous rocks may underplate the
425 continental crust and infiltrate the lower continental crust. The petrophysical parameters of hypothesis
426 H5 allowed us to adopt model geometries that matched the gravimetric and magnetic observations
427 better than the other hypotheses. The overall geometry and location of the large-scale magnetic body
428 remains similar regardless of the different lithologies. Hereafter the magnetic body generating the
429 CMA is called the Catalan body.

430 **5.2. Proposed 2D geophysical model**

431 Our model for cross-sections M1 and M2 (**Fig. 7**), described below, were obtained using
432 hypothesis H5. These sections are considered here as the final result of the modelling, as they best
433 match the magnetic and gravimetric data and fulfil reasonable geological hypotheses.

434 5.2.1. Section M1

435 Section M1 extends perpendicular to the GoL margin from the continental domain onshore to
436 the deep oceanic domain offshore (**Fig. 2**). In agreement with the SARDINIA and ECORS seismic
437 profiles, the Cenozoic sedimentary cover thickens from negligible at the coastline to 9 km thick at the
438 outer edge of domain I. The boundary between the upper and lower continental crust is at around 13
439 km depth, in accordance with the nearby SARDINIA seismic profile.

440 The regional gravity signature along this section fits a significant crustal thinning in two
441 necking zones that are linked to a rise in the mantle from 30 km to about 10 km deep over a horizontal
442 distance of 180 km. The first necking zone is under the western part of the Graben Central, i.e. the
443 Catalan basin, and the second one is under the continental slope of the GoL margin. Under the Catalan
444 basin, the gravity mass deficit imposed by the 6-km-thick sedimentary infill is compensated by a rise
445 in the Moho nearly to 15 km depth over a horizontal distance of 40 km.

446 Under the Rascasse horst, the Moho is deeper and thus a thicker crustal block is present in that
447 area (around 20 km). It is composed of upper continental crust (less than 10 km thick) and the Catalan
448 body. The lateral extent of the Catalan body corresponds to the width of the CMA.

449 The Catalan body is located at the top of the mantle in the necking area of the GoL margin (**Fig.**
450 **7**). Its fit with the CMA and gravity values indicates respectively that it must be a highly magnetized
451 body with low density contrast with its surroundings. In order to better approach the most probable
452 field conditions, we created a vertical gradient of density and magnetic susceptibility by dividing the
453 Catalan body into three distinct bodies (numbered 7, 8 and 9 in **Fig. 7**) with decreasing density and
454 magnetic susceptibility from bottom to top (see **Table 1**). The lower body is assigned a density typical
455 of gabbro, and the middle and upper bodies have the densities close to the densities assigned to the
456 lower and upper crust, respectively (**Table 1**). The Catalan body under the Rascasse horst coincide

457 with a deepening of the moho and a thickening of the crust. The shallower part of the Catalan body
458 contains two indentations to fit the two lobes of the magnetic high.

459 In the transitional domain (domain II, [Fig. 1](#)), gravimetric values imply an unusually dense
460 (3100 kg/m^3) and thin (2–3 km) crust between the sedimentary cover (2600 kg/m^3) and the mantle
461 (3360 kg/m^3). This ascribed density corresponds to neither typical lower continental crust (2950
462 kg/m^3) nor unaltered mantle material (3360 kg/m^3). Different hypotheses are made concerning its
463 nature, it could be 1) a hyperextended lower continental crust that is densified by mafic intrusions (e.g.
464 [Séranne et al., 1995](#); [Séranne, 1999](#); [Moulin et al., 2005, 2015](#); [Aslanian et al, 2009](#); [Jolivet et al.,](#)
465 [2015](#)); (2) an exhumed serpentized mantle ([Boillot et al., 1980, 1987, 1989](#); [Beslier et al., 1993](#)) or
466 (3) an atypical oceanic crust formed at a very slow spreading rate (e.g. [Dick et al., 2003](#); [Klimke et al.,](#)
467 [2016](#); [Sauter et al., 2016](#)). Strong debates are ongoing between the first two hypotheses. Recent
468 studies demonstrate the occurrence of important volcanic edifices and magmatic crust in the north of
469 the Valencia Basin close to the GoL transitional domain ([Jolivet et al., 2019](#); [Maillard et al., 2019](#)).
470 The most plausible hypothesis to us would be the hyperextended lower crust intruded by mafic
471 magmatic product with low magnetic susceptibility. The second hypothesis is possible but it seems
472 difficult to connect an exhumed serpentized mantle with the recent observed magmatic crust of the
473 Northern Valencia basin. A study and further discussion on the nature of the transitional crust is out of
474 the scope of this paper, interested readers are invited to refer to the quoted papers.

475 To summarize, cross-section M1 presents the geometry of a passive continental margin with
476 significant crustal thinning and a rise in the mantle in the necking zone, with a mafic magmatic
477 underplating and intruding the continental crust.

478 5.2.2. Section M2

479 Section M2 ([Fig. 7](#)) crosses the continental shelf of the GoL margin (domain I) from the eastern
480 Pyrenees to the Provence area ([Fig. 2](#)) and cuts through the CMA and anomaly B ([Fig. 5](#)). It crosses
481 the SARDINIA and ECORS seismic profiles and is located near the recent PYROPE onshore seismic
482 profiles, shown on the western edge of [Fig. 2](#) ([Diaz et al., 2018](#); [Wehr et al., 2018](#)). These seismic data
483 allowed us to constrain the thickness of the Cenozoic sedimentary cover, the boundary between upper
484 and lower continental crust, and the Moho depth.

485 The regional gravity signature along this section fits with a crust that thins from 30 km in the
486 Pyrenees to 12 km in the Catalan zone on one side, and from 35 km in the Provence margin to 12 km
487 in the Catalan zone on the other side. The crustal thinning is greater at a distance of about 80 km east
488 of the Pyrenees, where the corresponding depression is filled by a Tertiary sedimentary cover as thick
489 as 7 km. Note that the continental crust is thicker in the Provence margin than in the eastern Pyrenees.
490 Neither the lower nor the upper crustal layers have the same thicknesses on the opposite sides of the
491 section. On the west (Pyrenean) side, the boundary between the upper and lower crusts rises offshore
492 as the lower crust thins from 10 to 6 km. Inversely on the east (Provence) side, the boundary between
493 the upper and lower crust is fixed at a depth of 14 km, consistently with the SARDINIA and ECORS
494 seismic profiles. The crustal thinning on both sides is linked to a rise in the mantle to a depth of
495 around 20 km. The rise on the western side is smooth and regular (13 km over a horizontal distance of
496 180 km). On the eastern side, the Moho depth (rising by 16 km over 200 km) is based on many
497 published estimates, but it is poorly constrained by a lack of deep seismic data onshore in Provence.

498 The two distinct anomalies (CMA and anomaly B) along the M2 profile represent two different
499 magnetic bodies (**Fig. 7**). On the Pyrenees side, the position of the CMA confines the Catalan body
500 (20 km wide) to the west of the area of the greatest crustal thinning. Anomaly B is located east of the
501 thinnest crust in the GoL margin.

502 On section M2, the CMA is induced by the Catalan body, modelled as three superimposed
503 bodies with different magnetic susceptibilities (7, 8 and 9 in **Fig. 7**; **Table 1**). This body is very
504 narrow (20 km wide) and thick (12 km). The lowest, most intensely magnetized body is 2 km thick,
505 the middle one is 7 km thick and the upper one is 2 km thick. Anomaly B is induced by a small body
506 with the characteristics of magnetic body 7 that is 20 km wide and 2 km thick.

507 In brief, section M2 shows the transition between the Pyrenees and the GoL margin. This
508 transition is characterized by significant crustal thinning and a rise of the mantle, but also by the
509 presence of narrow bodies of mafic rocks flanking the area of maximum thinning.

510

511 **6. Moho topography**

512 **6.1. New Moho depth map**

513 A new map of Moho depth (**Fig. 8**) was computed during this study. The base map is an
514 unpublished compilation (G. Martelet, pers. comm.) of published data based on converted seismic
515 interpretations in the GoL (e.g. [Séranne, 1999](#); [Gallart et al., 2001](#); [Mauffret et al., 2001](#); [Nercessian et](#)
516 [al., 2001](#); [Gailler et al., 2009](#); [Moulin et al., 2015](#)). These data were complemented by Moho depths
517 observed on passive seismic profiles by [Diaz et al. \(2018\)](#) in the eastern Pyrenees and by depths
518 derived from the 3D model of [Wehr et al. \(2018\)](#), based on seismic interpretation and Bouguer
519 anomaly constraints. The Moho depths calculated from the chosen model of this study were also taken
520 into account. Moho isobaths, based on depths rounded to the nearest kilometre, were inferred from the
521 structural configuration of the margin and the thicknesses of the synrift and postrift sediments ([Gorini,](#)
522 [1993](#); [Guennoc et al., 1994](#); [Séranne, 1999](#); **Fig. 2**). The most recent data were favoured, however,
523 some areas where the connection between different datasets was not straightforward, we did not draw
524 any isobaths especially between the Catalan and Roussillon basins (Fig. 8A, discussion below). The
525 depth-to-Moho digital terrain model (colour field in **Fig. 8A**) is computed by interpolation between the
526 isobaths.

527 **6.2. Impact of the models on Moho topography**

528 In the eastern GoL, the Moho slopes upward evenly towards the toe of the margin. The Moho
529 depth decreases gradually from 25 to 20 km below the continental shelf and more steeply (from 20 to
530 14 km) below the continental slope and the necking zone. In contrast, the Moho topography is
531 irregular in the western GoL. There, the Moho is shallow, reaching 16 km depth below the Catalan
532 basin in the proximal part of the continental shelf. Because of the lack of data, we can neither validate
533 nor reject a possible structural and geometrical connection between the Catalan and Roussillon basins.
534 In this case, Moho isobaths are not drawn on the western side of the Catalan basin (Fig.8A).
535 Moreover, our models did not allow us to validate or discard the possible presence of the North
536 Pyrenean Fault in the Catalan basin or the Rascasse horst.

537 Section M1 and the SARDINIA and ECORS profiles parallel to it show significant thinning of
538 the continental crust linked to a rise in the mantle along the whole margin (**Fig. 8B**). Moho isobaths

539 (Fig. 8A) indicate a significant landward indentation in the western GoL margin. Here the Moho rises
540 from 30 km deep near the beginning of the hinge zone to less than 15 km in a more proximal area than
541 in the eastern GoL (below the continental shelf), and the Moho rise is steeper in section M1 than in the
542 SARDINIA (15 km to its east) and ECORS profiles (Fig. 8B). Section M1 shows that the boundary
543 between domains I and II is located at the same level as interpreted by Moulin *et al.* (2015) on the
544 SARDINIA profile.

545 In the Pyrenees-GoL transition, the Moho rises steeply from 25 to 15 km depth over a horizontal
546 distance of ~50 km northeast of the Cap de Creus (Fig. 8A). The map shows an abrupt margin
547 trending NW-SE. This orientation matches those of the CTZ, the shear zones of Cap de Creus and the
548 Figueres-Montgrí basin to its southwest (e.g. Carreras, 2001; Vissers *et al.*, 2016; Monié *et al.*, 2018;
549 Druguet *et al.*, 2018).

550

551 7. Discussion

552 The results of our 2D geophysical modelling provide new information on the origin of the CMA
553 and the transition between the Pyrenees and the GoL margin. They are discussed below in relation to
554 the geodynamic context.

555 7.1. The Catalan body

556 Modelling based on gravimetric and magnetic data implies the presence of a large mafic
557 magmatic body below the western GoL margin, called here the Catalan body, and a smaller one to its
558 east corresponding to anomaly B (Fig. 1 and Fig. 5 and profile M2 in Fig. 7). The Catalan body is
559 approximately 80 km long, 20 km wide, and 12 km thick and is oriented NW-SE. It is located in the
560 necking area of the GoL continental margin, but not in the thinnest continental crust area. Both bodies
561 have magnetic and gravimetric properties consistent with those of gabbroic rocks. Taking into account
562 the geometries and petrophysical characteristics of the models along our two profiles, we interpret the
563 Catalan body as a gabbroic magmatic body that underplates (body 7 in Fig. 7) and intrudes the thinned
564 lower and upper continental crust (bodies 8 and 9, respectively). Anomaly B is explained by the
565 presence of a smaller underplating mafic magmatic body (body 7).

566 The setting of the Catalan body can be explained by several hypotheses, proposed on the basis
567 of the regional geodynamic context.

568 One hypothesis is that the Catalan body is a mafic underplating and intruding the thinned
569 continental crust, like those observed on volcanic margins. However, the GoL doesn't show the main
570 features of a typical volcanic margin (Geoffroy *et al.*, 2005): no SDR (seaward-dipping reflector) has
571 been observed in the upper crust and most authors described the GoL as a nonvolcanic continental
572 margin (e.g. Séranne *et al.*, 1995; Séranne, 1999; Moulin *et al.*, 2005, 2015; Aslanian *et al.*, 2009;
573 Jolivet *et al.*, 2015). The Catalan body could be the product of basaltic melt intrusions into this margin
574 during the Oligo-Miocene extension and breakup of the continental lithosphere, by analogy to the
575 Northern Red Sea margin (Ligi *et al.*, 2018).

576 A second hypothesis is that the Catalan body is the product of back-arc volcanism along the
577 CTZ, coherent with proposed kinematic reconstructions (Jolivet *et al.*, 2015; Romany *et al.*, in prep;
578 Jolivet *et al.*, 2019). Indeed, magmatic bodies on the surrounding margins of southeastern France and
579 Corsica formed in the back-arc region of the retreating Apennine slab during the rotation of the
580 Corsica-Sardinia block (Jolivet & Faccenna, 2000; Rehault *et al.*, 2012). Transfer faults, which
581 accommodate different rates of extension, might have localized and constrained the emplacement of
582 these magmatic bodies. Indeed, the Catalan body is in the Catalan transfer zone (CTZ). The CTZ may
583 belong with the North Balearic transfer zone (NBTZ, Fig 1) to the same system, allowing the Corsica-
584 Sardinia block rotation and the opening of the Liguro-Provençal basin (Fig. 1).

585 A third hypothesis is that the magmatic material came from the magmatic province of northern
586 Valencia Trough described by Maillard *et al.* (2019) through the CTZ, which acted as a leaky
587 transform and localized the Catalan magmatic body. Indeed, volcanic and magmatic seamounts are
588 aligned along the transfer zones that segment the Valencia Trough (Fig. 1, Maillard *et al.*, 1992). In
589 the north eastern Valencia Trough, Maillard *et al.*, 2019 depicts a volcanic province where magmatic
590 formation can reach a 3 km thickness in a spreading zone above a thin and sheared crust, implying
591 high temperatures and ductile behaviour during rifting. This area is affected by the NBTZ. The Catalan
592 Body may be a magmatic body linked to the Valence magmatic province by the CTZ.

593 By analogy to the Vøring volcanic transform margin, a fourth hypothesis could be that the
594 magmatic material originated during transtension along a transfer fault (the CTZ in our case). Indeed
595 transtensional motion can open pull-apart basins and lead to crustal thinning that promotes melt
596 production (Berndt *et al.*, 2001; White & McKenzie, 1989; Pedersen & Skogseid, 1989). Berndt *et al.*
597 (2001) referred to such magmatic intrusions as “transform margin highs”. They have been reported in
598 multiple transition zones such as East Canada (Reid, 1989), the Exmouth Plateau (Lorenzo *et al.*,
599 1991; Lorenzo & Vera, 1992), the western Barents Sea margin (Våagnes, 1997) and the Côte d’Ivoire–
600 Ghana margin (Basile *et al.*, 1998). In agreement with this hypothesis, according to Mauffret *et al.*
601 (2001), extension related to transfer activity should not be confused with the normal extension
602 associated with horst and graben structures, suggesting that the Catalan basin could be formed during a
603 pull-apart motion. Moreover, the Moho map shows an abrupt margin trending NW-SE at the East of
604 Cap de Creus (Eastern Pyrenees), similar to the morphology of a transform margin highs.

605 On the basis of the regional geodynamic context, we propose that the setting-up of the Catalan
606 body was induced by a combination of these events. The slab retreat and the motion along transfer
607 zones during the opening of the Liguro-Provençal Basin lead to a continental crust thinning and
608 induced the production of hot and ductile material in this area. This magma followed the facilitated
609 paths created by the major crustal fault of the CTZ, maybe the fault n°1 described by Mauffret *et al.*
610 (2001) (see fig 2).

611 **7.2. Age of the Catalan body**

612 The question arises as to the history of the tectonic structures around the Catalan body. The
613 NW-SE-trending transfer zones or faults in the area could be reactivated structures inherited from the
614 Pyrenean collision, the Mesozoic rifting or the Hercynian orogeny. Indeed, reactivated Paleozoic and
615 Pyrenean shear zones with similar orientations are found in the Cap de Creus area (e.g. Carreras, 2001;
616 Vissers *et al.*, 2016; Monié *et al.*, 2018; Druguet *et al.*, 2018), and further south the Mesozoic
617 Figueres-Montgrí basin is also oriented NW-SE. Thus we cannot rule out the possibility that the
618 Catalan body was inherited from previous tectonic events. However, two facts weigh against this
619 possibility. Firstly, the orientation of the CMA is parallel and superimposed onto the CTZ which is
620 linked to the opening of the Liguro-Provençal Basin. Secondly, near the Catalan body and on adjacent

621 and conjugate margins (Valencia and Sardinia respectively), there is the occurrence of Miocene
622 volcanism (Jolivet *et al.*, 2015), induced by the slab retreat of the Apennines (Maillard *et al.*, 2019;
623 Jolivet *et al.*, 2019) dated to 30 Ma (e.g. Auzende *et al.*, 1973; Gattacceca *et al.*, 2007). On the
624 kinematic reconstruction, the volcanism of the SW Sardinia margin and the northern Valencia basin
625 fits with the Catalan body. Thus we favour an interpretation that involves underplating and intrusion of
626 mafic melt related to the transfer zone motion linked to the opening of the Liguro Provençal basin
627 associated with magmatism caused by back-arc extension.

628 **7.3. The Pyrenees – GoL margin transition**

629 From our new Moho depth map and models we show that the western part of the GoL margin
630 (from SARDINIA profile to the cap de Creus, ~50 km wide) is characterized by a heterogeneous
631 crustal structure (see the M1 and SARDINIA profiles in [Fig. 8B](#)). The thinned continental domain
632 (domain I) of this area is composed of (i) a thinned to hyper-thinned continental crust (25 to 0 km
633 thick), (ii) a rising mantle below thick Tertiary sedimentary sequences in the Catalan and Cathares
634 basins and (iii) the presence of a mafic magmatic body below the Rascasse horst. This deep structure
635 of the western side of the GoL margin (Cross-section M1 in [Fig. 7](#)) is not observed in the eastern part
636 of the GoL margin (ECORS profile in [Fig. 8](#)). To the east, crustal necking is in a more distal position,
637 tilted blocks are observed and even the thickness of the synrift deposits are uneven. The western
638 extremity of the GoL margin is bounded by a steep mantle rise at the toe of the Cap de Creus (eastern
639 Pyrenees; [Fig. 8A](#)).

640 We propose that this 50 km wide area is the marker of the CTZ, with many transfer faults as
641 suggested by Mauffret *et al.* (2001) (fault n°1 on [Fig 2](#)). The CTZ could extend further south,
642 according to [Mauffret *et al.* \(2001\)](#) and more recent seismic interpretations in the northern Valencia
643 Trough ([Maillard *et al.* 2019](#); [Jolivet *et al.*, 2019](#)).

644 The CTZ marks the transition from the Eastern Pyrenees to the GoL margin, which is not abrupt
645 but is a wide area. This transition would result from the transtensional motion along the transfer faults
646 of the CTZ and not only be linked to the rifting phase. The CTZ and the NBTZ belong to the same
647 transfer system that allowed the rotation of the Corsica-Sardinia block and the opening of the Liguro-
648 Provençal domain.

649 Even though the Tertiary formation of the Catalan basin, the CTZ and the Catalan magmatic
650 body are supposed to be coeval with the opening of the Liguro-Provençal Basin, we cannot rule out
651 the role of inherited structures from the Hercynian orogeny, Mesozoic rifting and Pyrenean orogeny in
652 explaining the crustal heterogeneity, transfer zones and Moho morphology of the GoL

653

654 **8. Conclusions**

655 To better characterize the transition between the Pyrenees and the Gulf of Lion (GoL) margin, a
656 wide range of available aeromagnetic and gravimetric data have been reprocessed to interpret of the
657 Catalan Magnetic Anomaly (CMA), the major high-amplitude magnetic anomaly of the GoL margin at
658 the foot of the eastern Pyrenees chain. We proceed to compute new RTP magnetic anomaly and
659 Bouguer anomaly maps, model the CMA from gravimetric and magnetic data and create a new Moho
660 depth compilation map.

661 From geophysical modelling along two perpendicular cross-sections, the CMA is interpreted as
662 a mafic magmatic body of significant dimensions ($80 \times 20 \times 12$ km), called the Catalan body. This
663 body underplates and intrudes the thinned continental crust in the necking zone of the western part of
664 the GoL margin along a crustal fault of the Catalan Transfer Zone (CTZ). We propose that this
665 magmatism was due to the transtensional motion along the CTZ, induced by the back-arc extension
666 above the retreating Apennine slab and thus produced during the Tertiary rifting phase of the Liguro-
667 Provençal Basin.

668 From the new compilation map of Moho depths, the 50 km-wide zone oriented NW-SE and
669 located in the western part of the GoL margin is attributed to the CTZ. The CTZ marks the transition
670 from the Pyrenean mountain belt to the GoL margin. It is characterized by a heterogeneous crustal
671 structure and Moho geometry: i) In the continental shelf, an important mantle rise is beneath the thick
672 Tertiary Catalan sedimentary basin (western part of the Graben Central); ii) The necking zone is more
673 proximal and steeper than that in the GoL margin at East; iii) The presence of the mafic magmatic
674 body in the thinned continental domain, certainly set up along a NW-SE crustal fault. The CTZ
675 belongs to the same transfer system as the NBTZ that allowed the rotation of the Corsica-Sardinia
676 block and the opening of the Liguro-Provençal domain.

677

678

679 **Acknowledgments:**

680 This study was carried out during the OROGEN project, funded by TOTAL, BRGM, and
681 INSU-CNRS. We thank the OROGEN's community for their helpful discussions. We are thankful for
682 the availability of the data accessible on the European Marine Observation and Data Network
683 Bathymetry portal (<http://www.emodnet-bathymetry.eu>) for the bathymetric metadata and digital
684 terrain model data products, and also for the BRGM's InfoTerre portal for the new geophysical
685 compilation (the gravimetric and magnetic database). We thank Andrew Alden for his proofreading
686 review, as well as the reviewers for their critical and constructive reviews.

687

688 **References**

689

690 Arthaud, F., Matte, P., 1975. Les décrochements tardi-hercyniens du sud-ouest de l'Europe. Géométrie
691 et essai de reconstitution des conditions de la déformation. *Tectonophysics* 25(1-2), 139-171.

692 Aslanian, D., Moulin, M., Olivet, J.-L., Unternehr, P., Bache, F., Rabineau, M., Matias, L., Nouzé, H.,
693 Klingelhofer, F., Contrucci, I., Labails, C., 2009. Brazilian and African passive margins of the
694 Central Segment of the South Atlantic Ocean: kinematic constraints. *Tectonophysics* 468, 98-
695 112.

696 Auzende, J.-M., Bonnin, J., Olivet, J.-L., 1973. The origin of the western Mediterranean basin. *J. Geol.*
697 *Soc., London* 129, 607-620.

698 Azambre, B., Pozzi, J.-P., 1982. Etude du magnétisme des roches éruptives de la région d'Arette
699 (Pyénées atlantiques), préliminaire à l'analyse de l'évolution des contraintes régionales. *Bull.*
700 *Soc. Géol. Fr.* 7(2), 255-263.

701 Bache, F., Olivet, J.-L., Gorini, C., Aslanian, D., Labails, C., Rabineau, M., 2010. Evolution of rifted
702 continental margins: The case of the Gulf of Lions (Western Mediterranean Basin). *Earth*
703 *Planet. Sci. Let.* 292, 345-356.

704 Bartrina, M.T., Cabrera, L., Jurado, M. J., Guimerà, J., Roca, E., 1992. Evolution of the central
705 Catalan margin of the Valencia trough (western Mediterranean). *Tectonophysics* 203(1-4), 219-
706 247.

707 Basile, C., Mascle, J., Benkhelil, J., Bouillin, K.-P., 1998. Geodynamic evolution of the Côte d'Ivoire-
708 Ghana Transform Margin: an overview of leg 159 results. *Proc. Ocean Drill. Program Sci.*
709 *Results* 159.

710 Bauer, K., Neben, S., Schreckenberger, B., Emmermann, R., Hinz, K., Fechner, N., Weber, K., 2000.
711 Deep structure of the Namibia continental margin as derived from integrated geophysical
712 studies. *J. Geophys. Res.* 105(B11), 25829-25853.

713 Benedicto, A., Labaume, P., Séguret, M., & Séranne, M. (1996). Low-angle crustal ramp and basin
714 geometry in the Gulf of Lion passive margin: Oligocene-Aquitainian Vistrenque graben, SE
715 France. *Tectonics*, 15(6), 1192-1212.

716 Bergerat, F., 1987. Stress fields in the European platform at the time of Africa-Eurasia collision.
717 *Tectonics* 6(2), 99-132.

718 Berndt, C., Mjelde, R., Planke, S., Shimamura, H., Faleide, J.I., 2001. Controls on the tectono-
719 magmatic evolution of a volcanic transform margin: the Voring Transform Margin, NE Atlantic.
720 *Mar. Geophys. Res.* 22, 133-152.

721 Beslier, M.-O., Ask, M., Boillot, G., 1993. Ocean-continent boundary in the Iberia abyssal plain from
722 multichannel seismic data. *Tectonophysics* 218, 383-393.

- 723 Bestani, L., Espurt, N., Lamarche, J., Floquet, M., Philip, J., Bellier, O., Hollender, F., 2015.
724 Structural style and evolution of the Pyrenean-Provence thrust belt, SE France. *Bull. Soc. Géol.*
725 *Fr.* 186(4-5), 223-241.
- 726 Boillot, G., Féraud, G., Recq, M., Girardeau, J., 1989. "Undercrusting" by serpentinite beneath rifted
727 margins: the examples of the west Galicia margin (Spain). *Nature* 341, 523-525.
- 728 Boillot, G., Grimaud, S., Mauffret, A., Mougénot, A., Kornbropst, J., Mergoïl-Daniel, J., Torrent, G.,
729 1980. Ocean-continent boundary off the Iberian margin: serpentinite diapir west of the Galicia
730 Bank. *Earth Planet. Sci. Lett.* 48, 23-34.
- 731 Boillot, G., Winterer, E.L., Meyer, A.W., 1987. Ocean Drilling Program. In: G. Boillot, E.L. Winterer
732 and A.W. Meyer, Eds, *Proc. Ocean Drill. Progr., Init. Repts.*, 103, 663pp. – College Station, TX:
733 Ocean Drilling Program.
- 734 Braun, J., Beaumont, C., 1989. A physical explanation of the relation between flank uplifts and the
735 breakup unconformity at rifted continental margins. *Geology* 17(8), 760-764.
- 736 Bridges, D., Mickus, K., Gao, S., Abdelsalam, M., Alemu, A., 2012. Magnetic stripes of a transitional
737 continental rift in Afar. *Geology* 40(3), 203-206.
- 738 Bronner, A., Sauter, D., Manatschal, G., Péron-Pinvidic, G., Munsch, M., 2011. Magmatic breakup
739 as an explanation for magnetic anomalies at magma-poor rifted margins. *Nature Geosc.*, 4(8),
740 549.
- 741 Buck, W.R., 2006. The role of magma in the development of the Afro-Arabian Rift System. *Geol.*
742 *Soc., London, Spec. Publ.* 259(1), 43-54.
- 743 Carreras, J., 2001. Zooming on Northern Cap de Creus shear zones. *J. Struct. Geol.* 23(9), 1457-1486.
- 744 Carreras, J., Druguet, E., Griera, A., Soldevila, J., 2004. Strain and deformation history in a
745 syntectonic pluton. The case of the Roses granodiorite (Cap de Creus, Eastern Pyrenees). *Geol.*
746 *Soc., London, Spec. Publ.* 224(1), 307-319.
- 747 Chamot-Rooke, N., Gaulier, J. M., Jestin, F., 1999. Constraints on Moho depth and crustal thickness in
748 the Liguro-Provençal basin from a 3D gravity inversion: geodynamic implications. *Geol. Soc.,*
749 *London, Spec. Publ.* 156(1), 37-61.
- 750 Chelalou, R., Nalpas, T., Bousquet, R., Prevost, M., Lahfid, A., Poujol, M., Ballard, J.F., 2016. New
751 sedimentological, structural and paleo-thermicity data in the Boucheville Basin (eastern North
752 Pyrenean Zone, France). *C. R. Geoscience* 348(3-4), 312-321.
- 753 Chevrot, S., Sylvander, M., Diaz, J., Martin, R., Mouthereau, F., Manatschal, G., Masini, E., Calassou,
754 S., Grimaud, F., Pauchet, H., Ruiz, M., 2018. The non-cylindrical crustal architecture of the
755 Pyrenees. *Scientific reports* 8(1), 9591. DOI:10.1038/s41598-018-27889-x
- 756 Choukroune, P., Mattauer, M., 1978. Tectonique des plaques et Pyrénées; sur le fonctionnement de la
757 faille transformante nord-pyrénéenne; comparaisons avec des modèles actuels. *Bull. Soc. Géol.*
758 *Fr.* 7(5), 689-700.

- 759 Choukroune, P., Seguret, M., Galdeano, A., 1973. Caractéristiques et évolution structurale des
760 Pyrénées. Un modèle de relations entre zone orogénique et mouvement des plaques. Bull. Soc.
761 Géol. Fr. S7-XV (5-6), 600-611.
- 762 Clerc, C., Lahfid, A., Monié, P., Lagabrielle, Y., Chopin, C., Poujol, M., de St Blanquat, M., 2015.
763 High-temperature metamorphism during extreme thinning of the continental crust: a reappraisal
764 of the North Pyrenean passive paleomargin. *Solid Earth* 6, 643-668.
- 765 Couëffé, R., Tourlière, B., Lasseur, E., Bauer, H., Beccaletto, L., Bialkowski, A., Briais, J., Capar, L.,
766 Paquet, F., Serrano, O., Thinon, I., 2016. Géométrie des bassins cénozoïques métropolitains :
767 premier aperçu fourni par la carte des épaisseurs de leur remplissage sédimentaire (projet
768 METROCENE). 25ème Réunion des Sciences de la Terre, 24-28 octobre 2016, Caen, Livre des
769 Résumés, pp. 64.
- 770 Diaz, J., Vergés, J., Chevrot, S., Antonio-Vigil, A., Ruiz, M., Sylvander, M., Gallart, J., 2018.
771 Mapping the crustal structure beneath the Eastern Pyrenees. *Tectonophysics* 744, 296-309.
- 772 Dick, H.J., Lin, J., Schouten, H., 2003. An ultraslow-spreading class of ocean ridge. *Nature*,
773 426(6965), 405.
- 774 Druguet, E., 2001. Development of high thermal gradients by coeval transpression and magmatism
775 during the Variscan orogeny: insights from the Cap de Creus (Eastern Pyrenees).
776 *Tectonophysics* 332(1-2), 275-293.
- 777 Druguet, E., Carreras, J., Mezger, J.E., 2018. Discussion on ‘Middle Jurassic shear zones at Cap de
778 Creus (eastern Pyrenees, Spain): a record of pre-drift extension of the Piemonte–Ligurian
779 Ocean?’ *Journal of the Geological Society, London*, 174, 289-300. *J. Geol. Soc.* 175(1), 187-
780 188.
- 781 Dunlop, D. J., Prévot, M., 1982. Magnetic properties and opaque mineralogy of drilled submarine
782 intrusive rocks. *Geophys. J. Int.* 69(3), 763-802.
- 783 Elo, S., 1997. Interpretations of the gravity anomaly map of Finland. *Geophysica* 33(1), 51-80.
- 784 Fournier, F., Tassy, A., Thinon, I., Münch, P., Cornée, J. J., Borgomano, J., Guennoc, P., 2016. Pre-
785 Pliocene tectonostratigraphic framework of the Provence continental shelf (eastern Gulf of Lion,
786 SE France). *Bull. Soc. Géol. Fr.* 187(4-5), 187-215.
- 787 Gailler, A., Klingelhoefer, F., Olivet, J. L., Aslanian, D., Technical, O.B.S., 2009. Crustal structure of
788 a young margin pair: new results across the Liguro–Provencal Basin from wide-angle seismic
789 tomography. *Earth Planet. Sci. Lett.* 286(1-2), 333-345.
- 790 Galdeano, A., Rossignol, J.-C., 1977. Contribution de l'aéromagnétisme à l'étude du Golfe de Valence
791 (Méditerranée Occidentale). *Earth Planet. Sci. Lett.* 34(1), 85-99.
- 792 Gallart, J., Diaz, J., Nercessian, A., Mauffret, A., Dos Reis, T., 2001. The eastern end of the Pyrenees:
793 Seismic features at the transition to the NW Mediterranean. *Geophys. Res. Lett.* 28, 2277-2280.

- 794 Gattacceca, J., Deino, A., Rizzo, R., Jones, D. S., Henry, B., Beaudoin, B., Vadeboin, F., 2007.
795 Miocene rotation of Sardinia: New paleomagnetic and geochronological constraints and
796 geodynamic implications. *Earth Planet. Sci. Let.* 258(3-4), 359-377.
- 797 Geoffroy, L., 2005. Volcanic passive margins. *Comptes Rendus Geoscience* 337(16), 1395-1408.
- 798 Geoffroy, L., Burov, E. B., & Werner, P. (2015). Volcanic passive margins: another way to break up
799 continents. *Scientific Reports*, 5, 14828.
- 800 Gorini, C., 1993. Géodynamique d'une marge passive : le Golfe du Lion (Méditerranée occidentale).
801 Thèse de doctorat, Université Paul Sabatier, Toulouse, 256 pp.
- 802 Gorini, C., Le Marrec, A., Mauffret, A., 1993. Contribution to the structural and sedimentary history
803 of the Gulf of Lions (western Mediterranean), from the ECORS profiles, industrial seismic
804 profiles and well data. *Bull. Soc. Géol. Fr.* 164(3), 353-363.
- 805 Gorini, C., Mauffret, A., Guennoc, P., Le Marrec, A., 1994. Structure of the Gulf of Lions
806 (northwestern Mediterranean Sea): A review. In: *Hydrocarbon and Petroleum Geology of*
807 *France* (pp. 223-243). Springer, Berlin, Heidelberg.
- 808 Granado, P., Urgeles, R., Sàbat, F., Albert-Villanueva, E., Roca, E., Muñoz, J.A., Gambini, R., 2016.
809 Geodynamical framework and hydrocarbon plays of a salt giant: the NW Mediterranean Basin.
810 *Petroleum Geoscience* 22(4), 309-321.
- 811 Gueguen, E., Doglioni, C., Fernandez, M., 1998. On the post-25 Ma geodynamic evolution of the
812 western Mediterranean. *Tectonophysics* 298, p. 259-269.
- 813 Guennoc, P., Debeglia, N, Gorini, C, Le Marrec, A, Mauffret, A., 1994. Anatomie d'une marge passive
814 jeune (Golfe du Lion - Sud France): apports des données géophysiques. *Bulletin des Centres de*
815 *Recherches Exploration-Production Elf Aquitaine* 18(1), 33-57.
- 816 Guennoc, P., Gorini, C., Mauffret, A., 2000. Histoire géologique du Golfe du Lion et cartographie du
817 rift oligo-aquitainien et de la surface messinienne. *Géol. Fr.* 3, 67-97.
- 818 Jolivet, L., Faccenna, C., 2000. Mediterranean extension and the Africa-Eurasia collision. *Tectonics*
819 19(6), 1095-1106.
- 820 Jolivet, L., Augier, R., Robin, C., Suc, J.-P., Rouchy, J.-M., 2006. Lithospheric-scale geodynamic
821 context of the Messinian salinity crisis. *Sed. Geol.* 188, 9-33.
- 822 Jolivet, L., Gorini, C., Smit, J., Leroy, S., 2015. Continental breakup and the dynamics of rifting in
823 back-arc basins: The Gulf of Lion margin. *Tectonics* 34(4), 662-679.
- 824 Jolivet L., Romagny A., Gorini C., Maillard A., Canva A., Thinon I., Coueffé R. and Peyrefitte A.,
825 2019. Post-orogenic evolution of Pyrenees and Liguro-Provençal rifting, the role of mantle flow.
826 Poster. *Geophysical Research Abstracts* Vol. 21, EGU2019-4033-1.
- 827 Kearey, P., Brooks, M., Hill, I., 2002. *An introduction to Geophysical Exploration*. Third edition.
828 Blackwell Science Ltd, 262 p.
- 829 Keen, C.E., Dickie, K., Dafoe, L.T., 2018. Structural characteristics of the ocean-continent transition
830 along the rifted continental margin, offshore central Labrador. *Mar. Petrol. Geol.* 89, 443-463.

- 831 Klimke, J., Franke, D., Gaedicke, C., Schreckenberger, B., Schnabel, M., Stollhofen, H., Chaheire, M.,
832 2016. How to identify oceanic crust - Evidence for a complex break-up in the Mozambique
833 Channel, off East Africa. *Tectonophysics* 693, 436-452.
- 834 Lagabrielle, Y., Bodinier, J.-L., 2008. Submarine reworking of exhumed subcontinental mantle rocks:
835 field evidence from the Lherz peridotites, French Pyrenees. *Terra Nova* 20(1), 11-21.
- 836 Lagabrielle, Y., Labaume, P., de Saint Blanquat, M., 2010. Mantle exhumation, crustal denudation,
837 and gravity tectonics during Cretaceous rifting in the Pyrenean realm (SW Europe): Insights
838 from the geological setting of the lherzolite bodies. *Tectonics* 29(4), TC4012
839 doi:10.1029/2009TC002588
- 840 Laske, G., Masters, G., Ma, Z., Pasyanos, M.E., 2012. CRUST1. 0: An updated global model of
841 Earth's crust. *Geophys. Res. Abs.* 14, 3743.
- 842 Lefebvre, D., 1981. Evolution morphologique et structurale du Golfe du Lion. Essai de traitement
843 statistique des données. Thèse de 3ème cycle, Paris VI, 163 pp.
- 844 Ligi, M., Bonatti, E., Bosworth, W., Cai, Y., Cipriani, A., Palmiotto, C., Seyler, M., 2018. Birth of an
845 ocean in the Red Sea: Oceanic-type basaltic melt intrusions precede continental rupture.
846 *Gondwana Res.* 54, 150-160.
- 847 Liotard, J. M., Maluski, H., & Dautria, J. M., 1991. Un Episode magmatique alcalin d'âge éocène en
848 Languedoc; la brèche volcanique de la montagne de la Moure (Hérault). *Bulletin de la Société*
849 *Géologique de France*, 162(6), 1067-1074.
- 850 Lorenzo, J. M. Vera, E.E., 1992. Thermal uplift and erosion across the continent-ocean transform
851 boundary of the southern Exmouth Plateau. *Earth Planet. Sci. Lett.* 108, 79-92.
- 852 Lorenzo, J. M., Mutter, J. C., Larson, R. L., Northwest Australia Study Group., 1991. Development of
853 the continent-ocean transform boundary of the southern Exmouth Plateau. *Geology* 19, 843-846.
- 854 Maffione, M., Morris, A., Plümpner, O., Van Hinsbergen, D.J.J., 2014. Magnetic properties of variably
855 serpentinized peridotites and their implication for the evolution of oceanic core complexes,
856 *Geochem. Geophys. Geosyst.* 15, 923-944. doi: 10.1002/2013GC004993.
- 857 Maillard, A., Mauffret, A., Watts, A. B., Torné, M., Pascal, G., Buhl, P., & Pinet, B., 1992. Tertiary
858 sedimentary history and structure of the Valencia trough (western
859 Mediterranean). *Tectonophysics*, 203(1-4), 57-75.
- 860 Maillard, A., 1993. Structure et riftogénèse du Golfe de Valence (Méditerranée occidentale). Thèse de
861 doctorat, Université Paris VI, 284 pp.
- 862 Maillard, A., Mauffret, A., 1993. Structure et volcanisme de la fosse de Valence (Méditerranée nord-
863 occidentale). *Bull. Soc. Géol. Fr.* 164(3), 365-383.
- 864 Maillard, A., Mauffret, A., 1999. Crustal structure and riftogenesis of the Valencia Trough (north-
865 western Mediterranean Sea). *Basin Res.* 11(4), 357-379.

- 866 Maillard, A., Gaullier, V., Vendeville, B. C., & Odonne, F. 2003. Influence of differential compaction
867 above basement steps on salt tectonics in the Ligurian-Provençal Basin, northwest
868 Mediterranean. *Marine and Petroleum Geology*, 20(1), 13-27.
- 869 Maillard A., Jolivet L., Thion I., Lofi J., Coueffé R. and Canva A. Accepted in 2019. Transfer Faults
870 and associated volcanic province in the Valencia Basin: consequences on crustal thinning.
871 *Marine and Petroleum Geology*.
- 872 Martelet, G., Debégliia, N., Truffert, C., 2002. Homogénéisation et validation des corrections de terrain
873 gravimétriques jusqu'à la distance de 167 km sur l'ensemble de la France, C. R. Geoscience
874 334, 449-454.
- 875 Martelet, G., Pajot, G., Debeglia, N., 2009. Nouvelle carte gravimétrique de la France; RCGF09–
876 Réseau et Carte Gravimétrique de la France, 2009. Rapport BRGM/RP-57908-FR, 77 pp.
- 877 Marti, J., Mitjavila, J., Roca, E., Aparicio, A., 1992. Cenozoic magmatism of the Valencia trough
878 (western Mediterranean): Relationship between structural evolution and volcanism.
879 *Tectonophysics* 203(1-4), 145-165. Doi: [https://doi.org/10.1016/0040-1951\(92\)90221-Q](https://doi.org/10.1016/0040-1951(92)90221-Q)
- 880 Mascle, A., Vially, R., Deville, E., Biju-Duval, B., Roy, J.-P., 1996. The petroleum evaluation of a
881 tectonically complex area: the western margin of the Southeast Basin (France). *Mar. Petrol.*
882 *Geol.* 13, 941-961.
- 883 Mauffret, A., Genneseaux, M., 1989. Compression, décrochement et distension sur le pourtour
884 méditerranéen nord-occidental. *C. R. Acad. Sci. Paris* 308, 961-967.
- 885 Mauffret, A., Maillard, A., Pascal, G., Torné, M., Buhl, P., Pinet, B., 1992. Long-listening
886 multichannel seismic profiles in the Valencia trough (Valsis 2) and the Gulf of Lions (ECORS):
887 a comparison. *Tectonophysics* 203(1-4), 285-304.
- 888 Mauffret, A., Pascal, G., Maillard, A., Gorini, C., 1995. Tectonics and deep structure of the north-
889 western Mediterranean Basin. *Mar. Petrol. Geol.* 12(6), 645-666.
- 890 Mauffret, A. & Gorini, C., 1996. Structural style and geodynamic evolution of Camargue and Western
891 Provençal basin, southeastern France. *Tectonics* 15, 356-375. doi:10.1029/95TC02407.
- 892 Mauffret, A., Durand de Grossouvre, B., Tadeu dos Reis, A., Gorini, C., Nercessian, A., 2001.
893 Structural geometry in the eastern Pyrenees and western Gulf of Lion (Western Mediterranean).
894 *J. Struct. Geol.* 23, 1701-1726.
- 895 Miller, D.J., Christensen, N.I., 1997. Seismic velocities of lower crustal and upper mantle rocks from
896 the slow-spreading mid-Atlantic ridge, South of the Kane Transform zone (MARK), in
897 *Proceeding of the Ocean Drilling Program, Scientific Results*, vol. 153, 437–454, Ocean Drill.
898 *Program*, College Station, Tex., doi:10.2973/odp.proc.sr.153.043.1997.
- 899 Monié, P., Oliot, E., Faucher, A., Allard, M., 2018. Age Eocène $^{40}\text{Ar}/^{39}\text{Ar}$ des zones de cisaillement de
900 basse température dans la péninsule du Cap de Creus (NW Espagne). Conséquences
901 géodynamiques. Talk. Congrès Réunion des Sciences de la Terre RST 26th edition. Lille.

- 902 Abstract p.234. <https://rst2018->
903 [lille.sciencesconf.org/data/book_rst2018_lille_fr_final_DEF_web.pdf](https://rst2018-lille.sciencesconf.org/data/book_rst2018_lille_fr_final_DEF_web.pdf)
- 904 Moulin, M., Aslanian, D., Olivet, J.-L., Contrucci, I., Matias, L., Géli, L., Klingelhoefer, F., Nouzé,
905 H., Réhault, J.-P., Unternehr, P., 2005. Geological constraints on the evolution of the Angolan
906 margin based on reflection and refraction seismic data ZaiAngo project. *Geophys. J. Int.* 162,
907 793-810.
- 908 Moulin, M., Klingelhoefer, F., Afilhado, A., Aslanian, D., Schnurle, P., Nouzé, H., Feld, A., 2015.
909 Deep crustal structure across a young passive margin from wide-angle and reflection seismic
910 data (The SARDINIA Experiment)–I. Gulf of Lion’s margin. *Bull. Soc. Géol. Fr.* 186(4-5),
911 309-330.
- 912 Nercessian, A., Mauffret, A., Dos Reis, A. T., Vidal, R., Gallart, J., Diaz, J., 2001. Deep reflection
913 seismic images of the crustal thinning in the eastern Pyrenees and western Gulf of Lion. *J.*
914 *Geodynamics* 31(2), 211-225.
- 915 Neres, M., Terrinha, P., Custódio, S., Silva, S.M., Luis, J., Miranda, J.M., 2018. Geophysical evidence
916 for a magmatic intrusion in the ocean-continent transition of the SW Iberia margin.
917 *Tectonophysics* 744, 118-133.
- 918 Olivet, J.-L., 1996. Kinematics of the Iberian plate. *Bulletin des Centres de Recherches Exploration-*
919 *Production Elf Aquitaine* 20(1), 131-195.
- 920 Oudet, J., Münch, P., Borgomano, J., Quillevere, F., Melinte-Dobrinescu, M.C., Demory, F., Cornee,
921 J.-J., 2010. Land and sea study of the northeastern golfe du Lion rifted margin: the Oligocene–
922 Miocene of southern Provence (Nerthe area, SE France). *Bull. Soc. Géol. Fr.* 181(6), 591-607.
- 923 Pascal, G.P., Mauffret, A., Patriat, P., 1993. The ocean-continent boundary in the Gulf of Lion from
924 analysis of expanding spread profiles and gravity modelling. *Geophys. J. Int.* 113, 701-726.
- 925 Pedersen, T., Skogseid, J., 1989. Vøring Plateau volcanic margin: Extension, melting and rifting, *Proc.*
926 *Ocean Drill. Program Sci. Results*, 104, p00-01.
- 927 Réhault, J.-P., Boillot, G., Mauffret, A., 1984. The Western Mediterranean basin geological evolution.
928 *Mar. Geol.* 55, 447-477.
- 929 Réhault, J.-P., Honthaas, C., Guennoc, P., Bellon, H., Ruffet, G., Cotten, J., Maury, R.C., 2012.
930 Offshore Oligo-Miocene volcanic fields within the Corsica-Liguria Basin: Magmatic diversity
931 and slab evolution in the western Mediterranean Sea. *J. Geodynamics* 58, 73-95.
- 932 Reid, I.D., 1989. Effects of lithospheric flow on the formation and evolution of a transform margin.
933 *Earth Planet. Sci. Lett.* 95, 38-52.
- 934 Rollet, N., Déverchère, J., Beslier, M.O., Guennoc, P., Réhault, J.-P., Sosson, M., Truffert, C., 2002.
935 Back-arc extension, tectonic inheritance, and volcanism in the Ligurian Sea, western
936 Mediterranean. *Tectonics* 21 (3), 218-243.

- 937 Sauter, D., Unternehr, P., Manatschal, G., Tugend, J., Cannat, M., Le Quellec, P., Granath, J.W., 2016.
938 Evidence for magma entrapment below oceanic crust from deep seismic reflections in the
939 Western Somali Basin. *Geology* 44(6), 407-410.
- 940 Schärer, U., Kornprobst, J., Beslier, M.O., Boillot, G., Girardeau, J., 1995. Gabbro and related rock
941 emplacement beneath rifting continental crust: UPb geochronological and geochemical
942 constraints for the Galicia passive margin (Spain). *Earth Planet. Sci. Lett.* 130(1-4), 187-200.
- 943 Schettino, A., Turco, E., 2006. Plate kinematics of the Western Mediterranean region during the
944 Oligocene and Early Miocene. *Geophysical Journal International*, 166(3), 1398-1423.
- 945 Séranne, M., 1999. The Gulf of Lion continental margin (NW Mediterranean) revisited by IBS: an
946 overview. In: "The Mediterranean Basins: Tertiary Extension within the Alpine Orogen ",
947 Durand, B., Jolivet, L., Horvatn, E., Séranne, M. (eds). Geological Society, London, Special
948 Publications, vol. 156, p. 15-36.
- 949 Séranne, M., Benedicto, A., Labaume, P., Truffert, C., Pascal, G., 1995. Structural style and evolution
950 of the Gulf of Lion Oligo-Miocene rifting: role of the Pyrenean orogeny. *Mar. Petrol. Geol.*
951 12(8), 809-820.
- 952 Shive, P.N., Frost, B.R., Peretti, A., 1988. The magnetic properties of metaperidotitic rocks as a
953 function of metamorphic grade: implications for crustal magnetic anomalies. *J. Geophys. Res.*
954 93(B10), 12187-12195.
- 955 Sibuet, J.C., Srivastava, S., Manatschal, G., 2007. Exhumed mantle-forming transitional crust in the
956 Newfoundland-Iberia rift and associated magnetic anomalies. *J. Geophys. Res.* 112(B6),
957 B06105 doi:10.1029/2005JB003856.
- 958 Tavani, S., Bertok, C., Granado, P., Piana, F., Salas, R., Vigna, B., Munoz, J.A., 2018. The Iberia-
959 Eurasia plate boundary east of the Pyrenees. *Earth-Science reviews* 187, 314-337.
- 960 Teixell, A., Labaume, P., Lagabrielle, Y., 2016. The crustal evolution of the west-central Pyrenees
961 revisited: Inferences from a new kinematic scenario. *C. R. Geoscience* 348(3-4), 257-267.
- 962 Telford, W.M., Geldart, L.P., Sheriff, R.E., Keys, D.A., 1984. *Applied Geophysics*. Cambridge
963 University Press, 860 pp.
- 964 Thybo, H., Artemieva, I.M., 2013. Moho and magmatic underplating in continental lithosphere.
965 *Tectonophysics* 609, 605-619.
- 966 Tugend, J., Manatschal, G., Kuszniir, N. J., Masini, E., Mohn, G., Thion, I., 2014. Formation and
967 deformation of hyperextended rift systems: Insights from rift domain mapping in the Bay of
968 Biscay-Pyrenees. *Tectonics* 33(7), 1239-1276.
- 969 Vågnes, E., 1997. Uplift at thermo-mechanically coupled ocean continent transforms: Modeled at the
970 Senja Fracture Zone, southwestern Barents Sea. *Geo-Mar. Lett.* 17, 100-109.
- 971 Vergés, J., Fernández, M., Martínez, A., 2002. The Pyrenean orogen: pre-, syn-, and post-collisional
972 evolution. *Journal of the Virtual Explorer* 8, 55-74.

- 973 Vielzeuf, D., Kornprobst, J., 1984. Crustal splitting and the emplacement of Pyrenean Iherzolites and
974 granulites. *Earth Planet. Sci. Lett.* 67(1), 87-96.
- 975 Vissers, R.L., Van Hinsbergen, D.J., Wilkinson, C.M., Ganerød, M., 2016. Middle Jurassic shear
976 zones at Cap de Creus (eastern Pyrenees, Spain): a record of pre-drift extension of the
977 Piemonte–Ligurian Ocean? *J. Geol. Soc., London* 174(2), 289-300.
- 978 Wang, Y., Chevrot, S., Monteiller, V., Komatitsch, D., Mouthereau, F., Manatschal, G., Benahmed, S.,
979 2016. The deep roots of the western Pyrenees revealed by full waveform inversion of
980 teleseismic P waves. *Geology* 44(6), 475-478.
- 981 Wehr, H., Chevrot, S., Courrioux, G., Guillen, A., 2018. A three-dimensional model of the Pyrenees
982 and their foreland basins from geological and gravimetric data. *Tectonophysics* 734-735, 16-32.
- 983 Wernicke, B., 1985. Uniform-sense normal simple shear of the continental lithosphere. *Can. J. Earth*
984 *Sci.* 22, 22.108-22.125.
- 985 White, R.S., McKenzie, D., 1989. Magmatism at rift zones: The generation of volcanic continental
986 margins and flood basalts. *J. Geophys. Res.* 94(B6), 7685-7729.
- 987 White, R.S., Spence, G.D., Fowler, S.R., McKenzie, D.P., Westbrook, G.K., Bowen, A.N., 1987.
988 Magmatism at rifted continental margins. *Nature* 330(6147), 439.
- 989 Ziegler, P.A., 1992. European Cenozoic rift system. *Tectonophysics* 208(1-3), 91-111.

990 **Figure captions**

991 **Fig. 1.** Magnetic anomaly map of the northwestern Mediterranean Sea showing the location of the
 992 Gulf of Lion (GoL) (after Galdeano & Rossignol, 1977 and Schettino & Turco, 2006). Note the major
 993 magnetic anomaly in the SW part of the GoL. Grey lines mark the boundaries of the continental,
 994 transitional and oceanic domains from Gailler *et al.* (2009). The rectangle outlines the study area (see
 995 **Fig. 3**).

996 **Fig. 2.** Structural setting of the GoL margin and surrounding area. Black lines represent the ECORS,
 997 SARDINIA and LRM10 seismic profiles (see **Fig. 3**), the PYROPE E-W profile (Diaz *et al.*, 2018),
 998 and sections M1 and M2 of this study (see **Fig. 7**). The location of the CMA is shaded in light pink.
 999 Heavy grey dashed lines are boundaries between crustal domains I, II and III from Gailler *et al.*
 1000 (2009). Transfer zones are only approximately located; the transfer zone labeled “1” is a hypothesized
 1001 en echelon fault related to the Catalan transfer zone from Mauffret *et al.* (2001). Dark grey
 1002 areas represent volcanic edifices. Offshore petroleum wells: Am, Agde Maritime; Au, Autan; Ca,
 1003 Calmar; Ci, Cincindele; GLP1/GPL2, Golfe du Lion Profond 1/2; Mi, Mistral; Ra, Rascasse; Si,
 1004 Sirocco; Tr, Tramontane. Mesozoic basins: Ag, Bas Agly basin; Bc, Boucheville basin; Bs, Beausset
 1005 syncline; FM, Figueres-Montgrís basin; SPF, St. Paul de Fenouillet. The inset map shows major
 1006 regional geological domains and structures (modified from Gorini *et al.*, 1993 edited by Séranne,
 1007 1999). Dotted areas represent the oceanic domain (Langhian–Serravalian), crosshatching the Alpine
 1008 orogen (Pliocene–Recent), dark grey the west European rift (Rupelian), and light grey the Pyrenean
 1009 orogen (Eocene). Green dashed line, limit between two domains of different shallow crustal structures.

1010 **Fig. 3.** Schematic sections from the (A) ECORS, (B) SARDINIA and (C) LRM10 interpreted seismic
 1011 profiles across the GoL margin (modified from Moulin *et al.* (2015), Séranne (1999) and Mauffret *et*
 1012 *al.* (2001), respectively). Only the boundaries of the different layers used for modelling are drawn. The
 1013 continental margin is divided into the continental domain (hinge zone, domain I), the transitional
 1014 domain (domain II) and the oceanic domain (domain III). The intersection with cross-section M2 is
 1015 shown. Triangles indicate projected locations of petroleum wells. LC, lower continental crust; OC,
 1016 oceanic crust; UC, upper continental crust, PQ, plio-quaternary; M, miocene; S, synrift deposit; PB,
 1017 paleozoic basement. CC: continental

1018 **Fig. 4.** Complete Bouguer anomaly map of the study area; the inset map shows the coverage of the
 1019 data used. The Bouguer reduction density used is 2300 kg/m³. Also shown are the SARDINIA and
 1020 ECORS seismic profiles and profiles M1 and M2 of this study. Note the gravimetric signals of a
 1021 granitic pluton (GS) sampled by the Sirocco well and the NE-SW Nîmes fault. The inset shows the
 1022 coverage of the gravimetric dataset: BGF and CGG gravity seafloor datasets (green), BGI (grey),
 1023 IFREMER-SISMER (blue) and Elf-Explo-1996 (purple).

1024 **Fig. 5.** RTP magnetic anomaly map of the study area. The CMA is the large positive feature in the
 1025 western part of the GoL margin coinciding with the M1 and SARDINIA profiles. The smaller anomaly
 1026 to its east is anomaly B (located by the letter B).

1027 **Fig. 6.** Schematic diagram of geometric modelling. (A) Observed (bold curve) and modelled (thin
 1028 curve) magnetic signals. (B) Observed and modelled gravimetric signals. (C) Model consisting of five
 1029 layers representing water, sedimentary cover, upper crust, lower crust and mantle with their associated
 1030 densities (kg/m^3).

1031 **Fig. 7.** Proposed geophysical models M1 and M2, based on hypothesis H5 (**Table 1**). Locations in
 1032 **Figs. 2** and **6**. Densities (ρ) are in kg/m^3 and magnetic susceptibilities (k) in SI. Materials 1 through 10
 1033 are as follows: 1, water layer ($\rho = 2300$; $k = 0$); 2, sedimentary cover ($\rho = 2350, 2400, 2600$; $k = 0$); 3,
 1034 upper continental crust ($\rho = 2700, 2750$; $k = 0$); 4, lower continental crust ($\rho = 2950$; $k = 0$); 5, mantle
 1035 ($\rho = 3360$; $k = 0$); 6, oceanic crust ($\rho = 2850$; $k = 0$); 7, lower part of the Catalan body ($\rho = 3100$; $k =$
 1036 0.11); 8, middle part of the Catalan body; ($\rho = 3000$; $k = 0.1$); 9, upper part of the Catalan body ($\rho =$
 1037 2800 ; $k = 0.06$); 10, transitional domain ($\rho = 3100$; $k = 0$). Main crustal domains of the GoL margin
 1038 are drawn. The crossings between M1, M2 and SARDINIA, ECORS and PYROPE seismic profiles
 1039 are indicated. The zero points in sections M1 and M2 correspond to the coasts of France and Spain,
 1040 respectively.

1041 **Fig. 8.** (A) Map showing Moho depth in the study area, compiled from the geophysical models of this
 1042 study and previously published data. Dashed isobaths are from 3D geological modelling of *Wehr et al.*
 1043 (2018); dot-dashed isobaths are compiled from *Mauffret et al. (1995)*, *Gallart et al. (2001)*, *Nercessian*
 1044 *et al. (2001)*, *Mauffret et al. (2001)*, *Gailler et al. (2009)*, *Diaz et al. (2018)*, and others; solid isobaths
 1045 are from this study. Question marks on where the connection between datasat was not straight
 1046 forward. Grey areas represent the extent and thickness of the magnetic body of mafic rocks that
 1047 generates the CMA. Hatched lines represent the transfer zones shown in **Figs. 1** and **2**. Note the
 1048 northward mantle indentation between the M1 section and the ECORS profile. The lateral extension of
 1049 the CTZ is represented by a red bracket. RB: Roussillon basin and CB: Catalan basin (B) ECORS and
 1050 SARDINIA profiles and section M1 aligned on their crossing with section M2. Blue crosses and lines
 1051 represent the location where the Moho rises to 15 km depth. See figure 2 for the precise location of the
 1052 Catalan and Cathare basins and the Rascasse horst.

1053 **Table 1.** Parameter values used for modelling, according to realistic geological assumptions.
 1054 Petrophysical values are inspired by *Telford et al. (1984)*, *Guennoc et al. (1994)*, *Berndt et al. (2001)*,
 1055 *Kearey et al. (2002)*, *Keen et al. (2018)* and *Neres et al. (2018)*. Gradients are modelled by the use of
 1056 multiple layers.

Figures

Figure 1

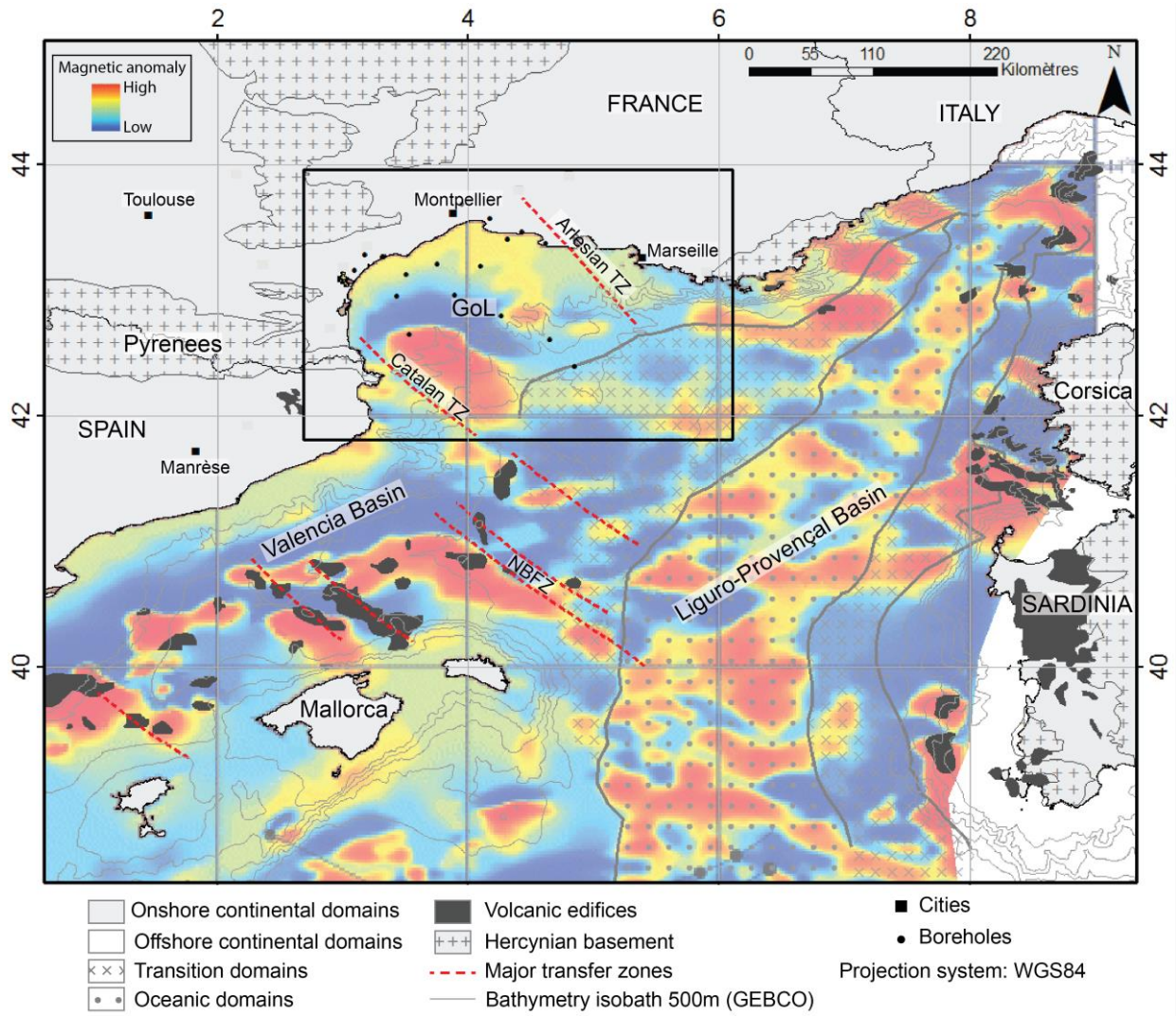


Figure 2

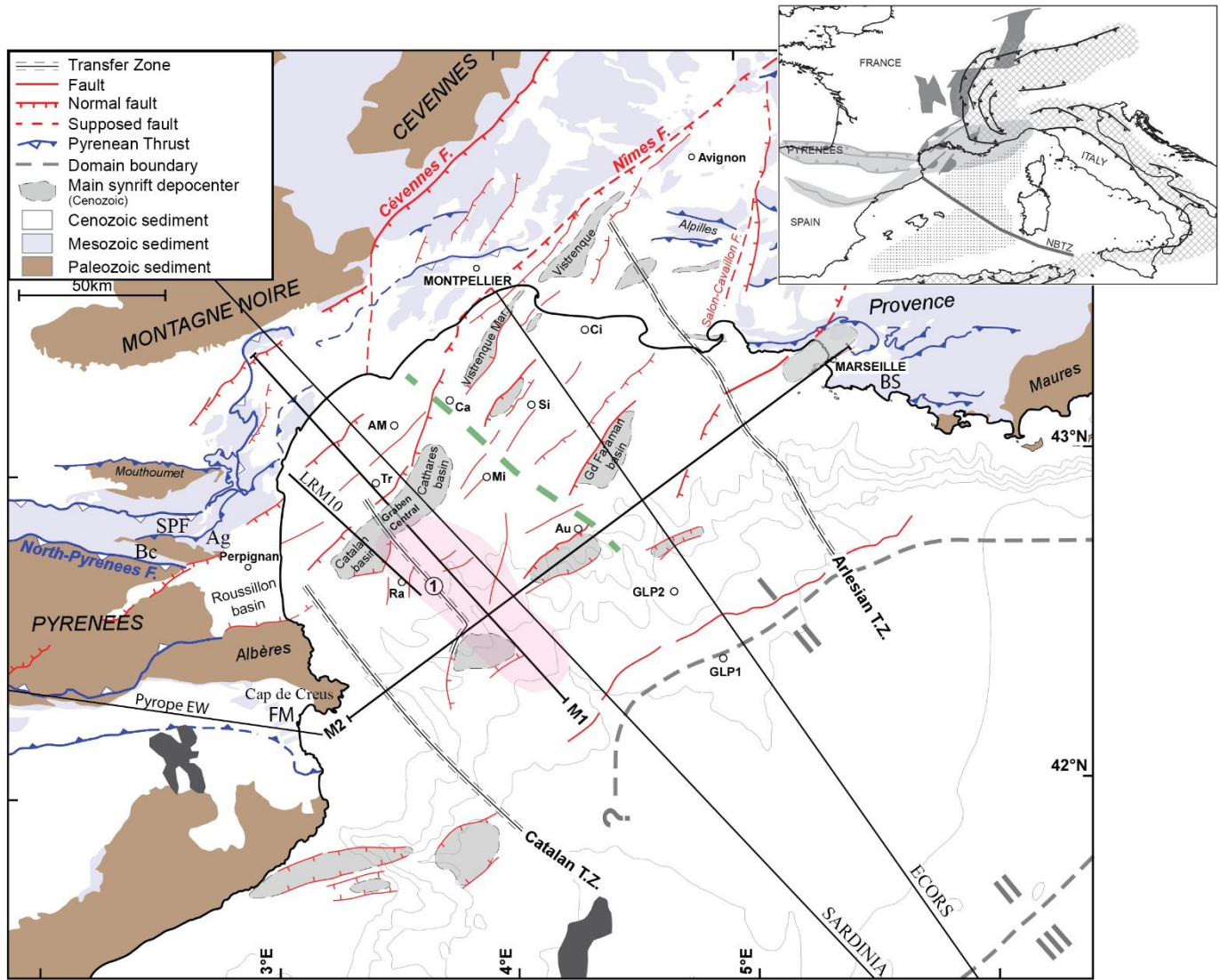


Figure 3

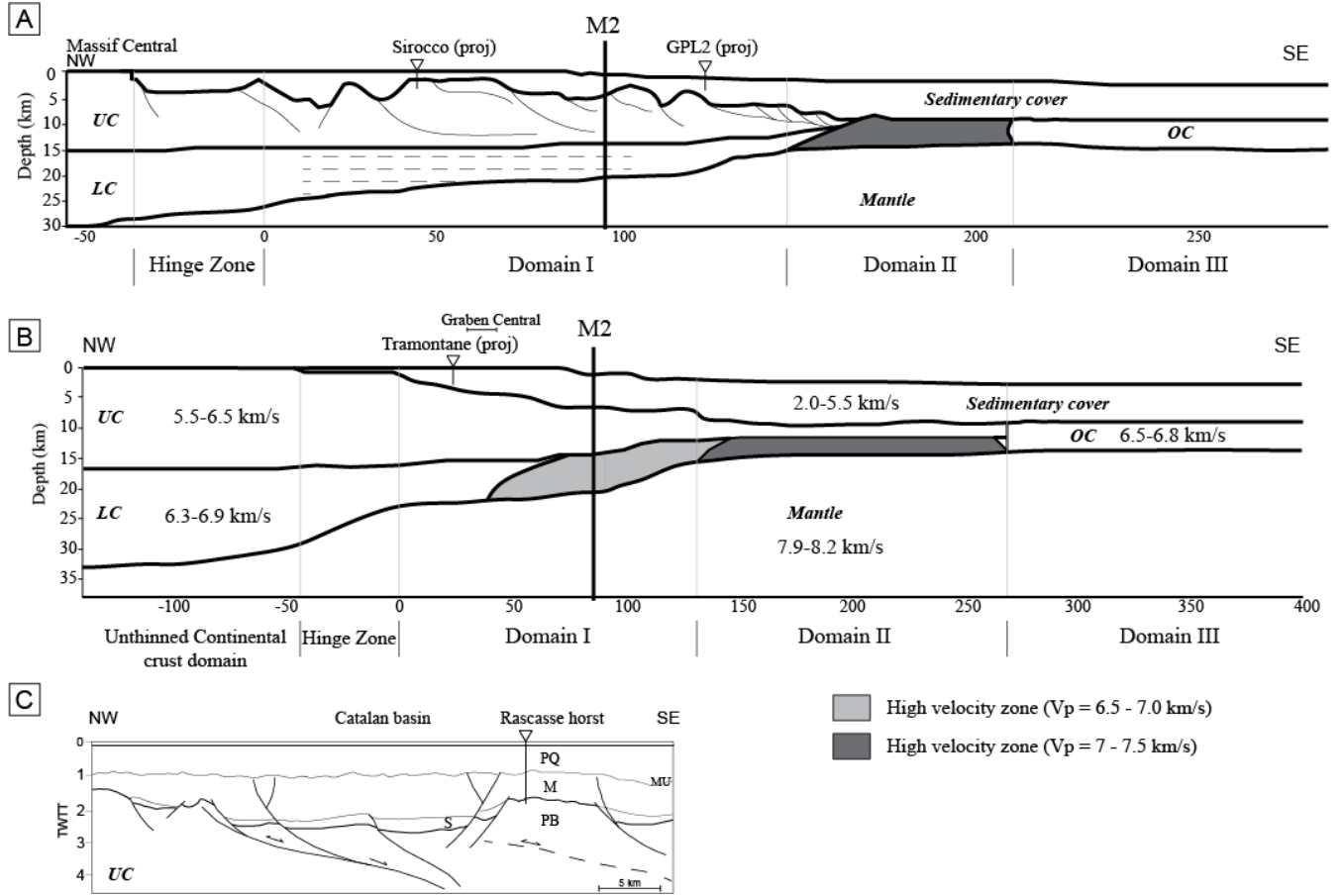


Figure 4:

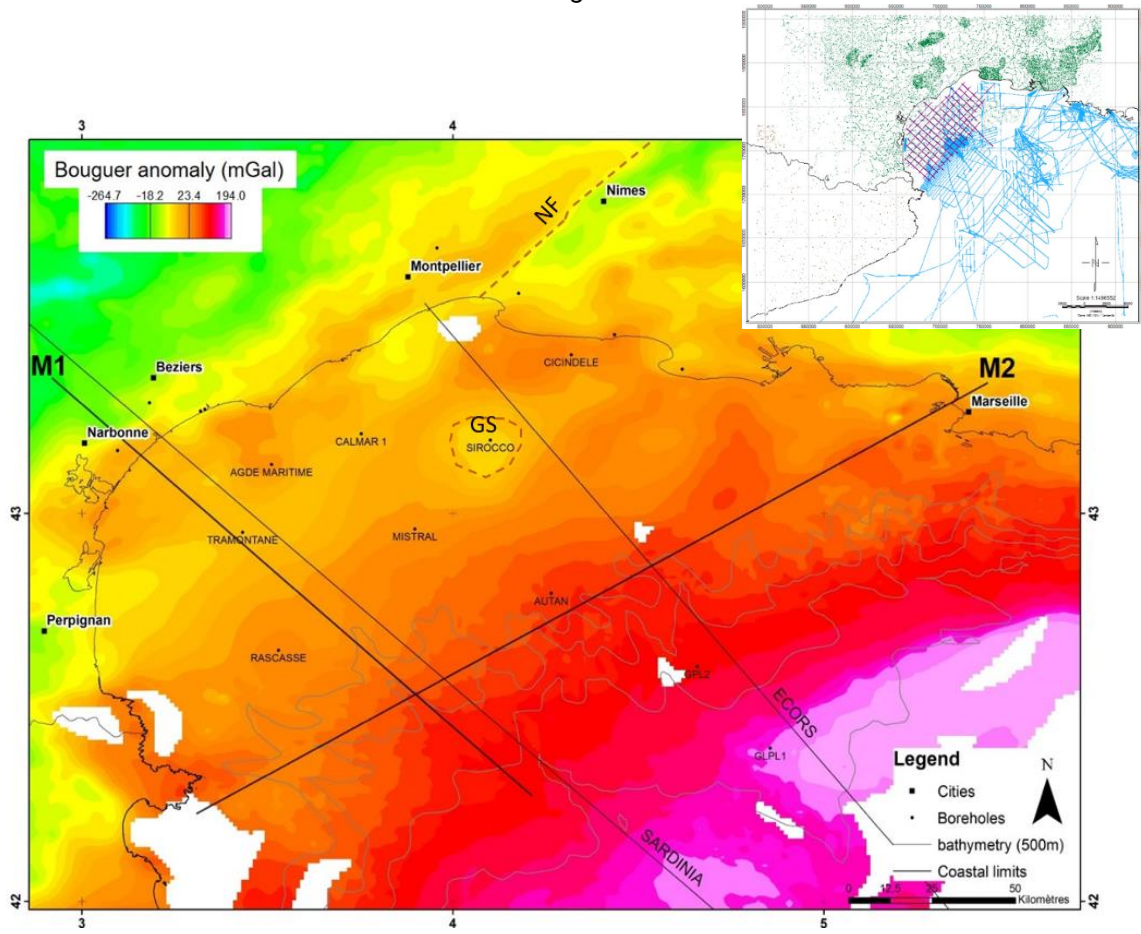


Figure 5

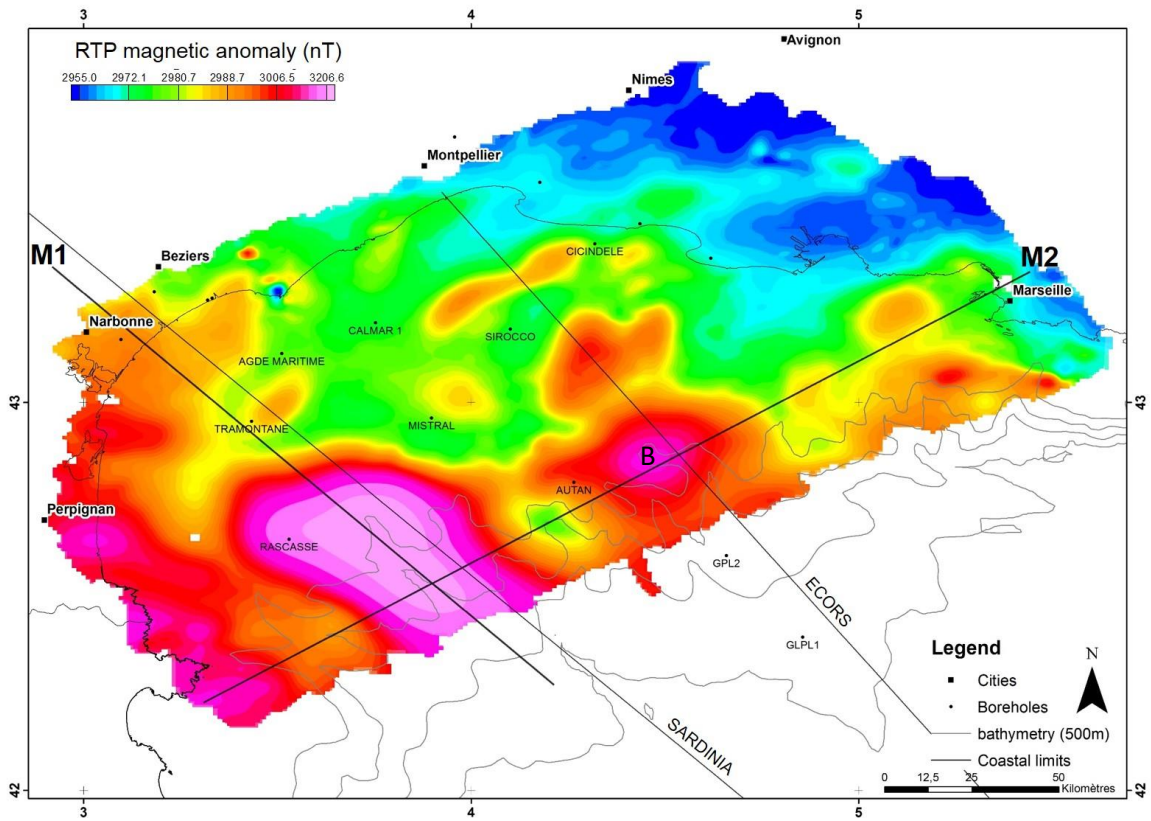


Figure 6

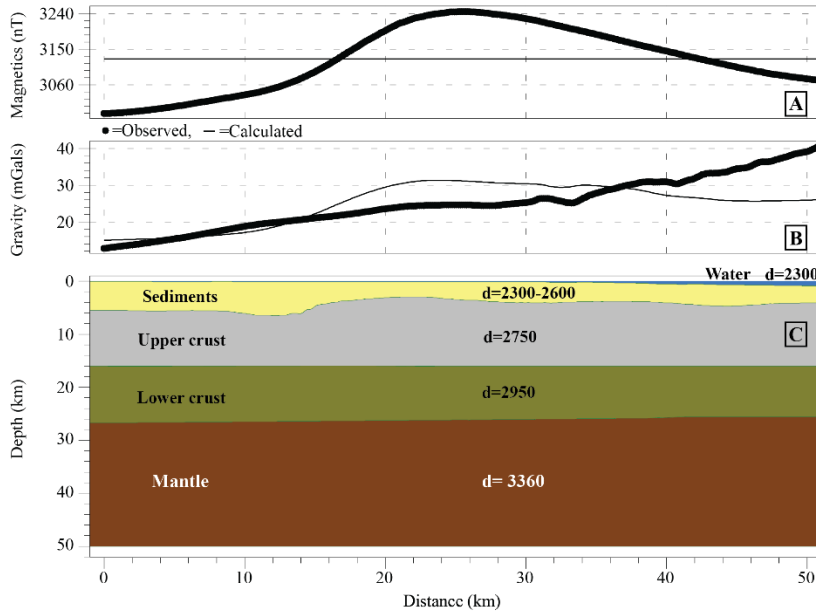


Table 1.—

Hypotheses		Density (Kg/m ³)	Magnetic Susceptibility (SI)	Maximum thickness (km)	Adjusted with the data	
					Magnetic	Gravimetric
H1	Basalt at the top of the upper crust	2850	0.18	4	~	x
H2	Basalt (1) at the top of the upper crust and gabbro (2) into the lower crust	(1) 2850 (2) 3000	0.15 0.10	4.5 5	~	x
H3	Basalt at the limit between the two crust	2850	0.1	8	√	x
H4	Gabbro between the upper crust and the mantle	3000	0.1	10	√	x
H5	Gabbro between the upper crust and the mantle with a petrophysical gradient (from top to bottom)	2800 3000 3100	0.06 0.1 0.11	2 7 2	√	√
H6	Serpentinized mantle	2700	0.1	10	√	x
H7	Serpentinized mantle, with a petrophysical gradient (from top to bottom)	2700 2850 2900 3000	0.3 0.15 0.09 0.005	>1 2 5 2.2	√	x

Figure 7

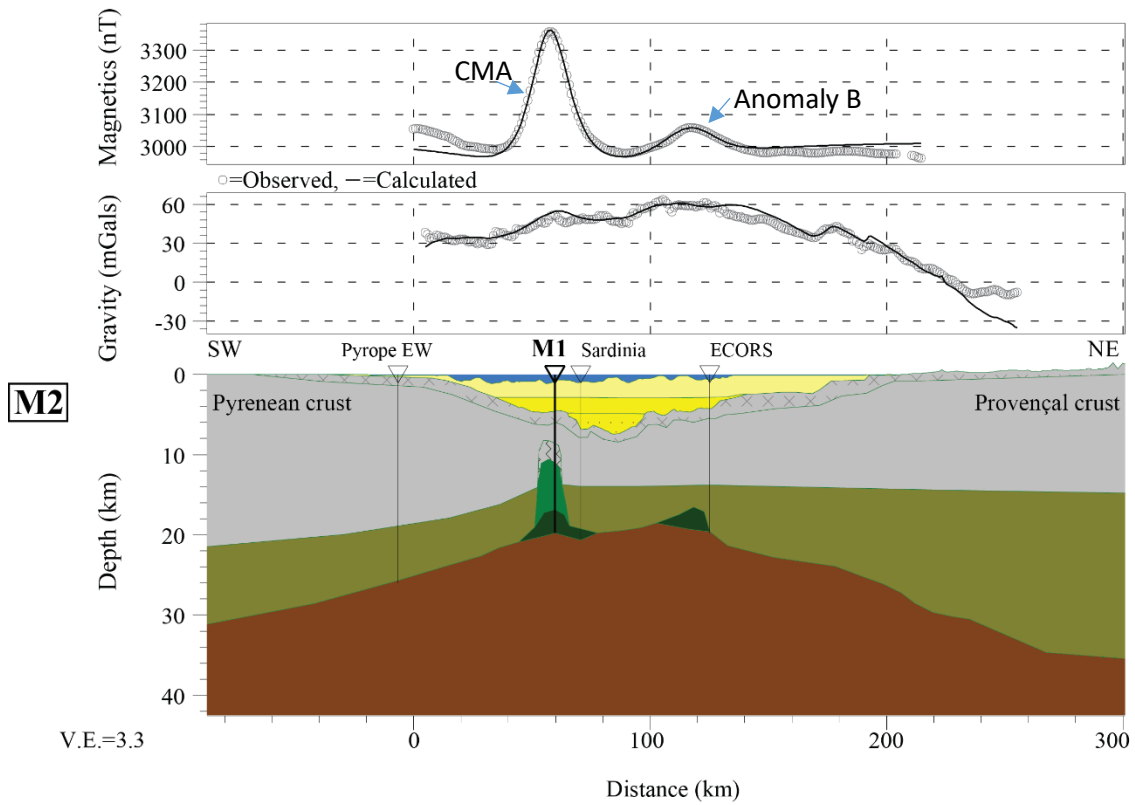
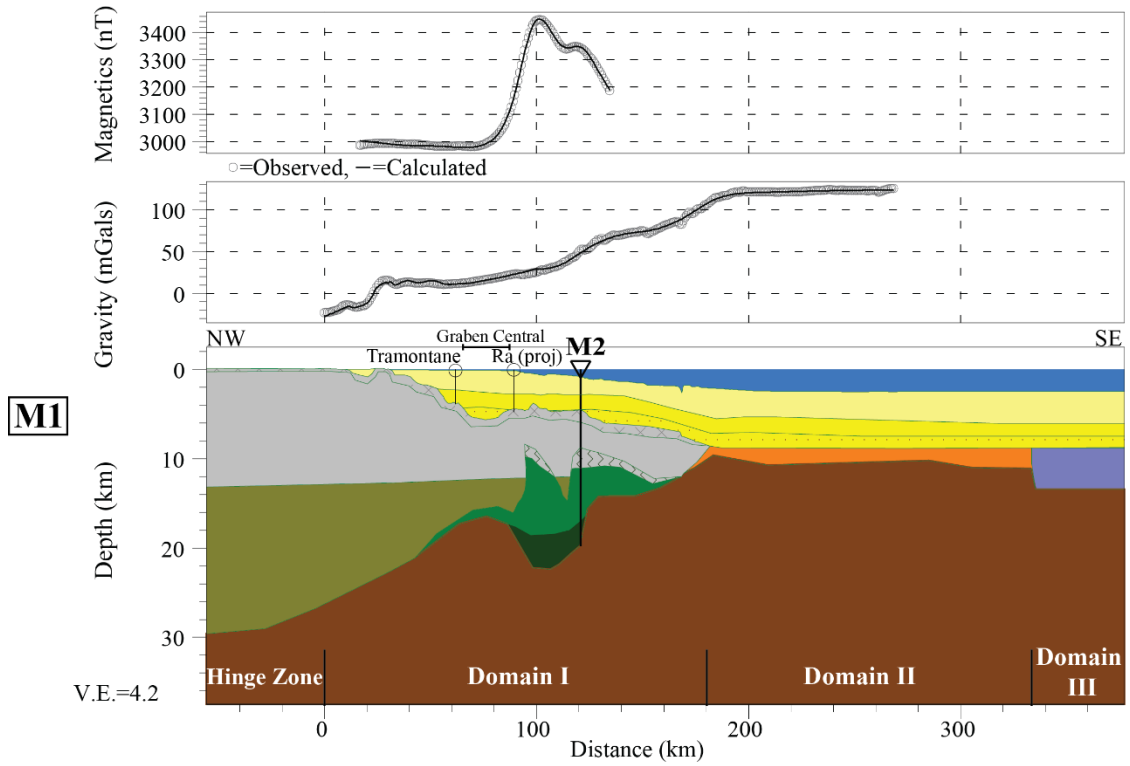
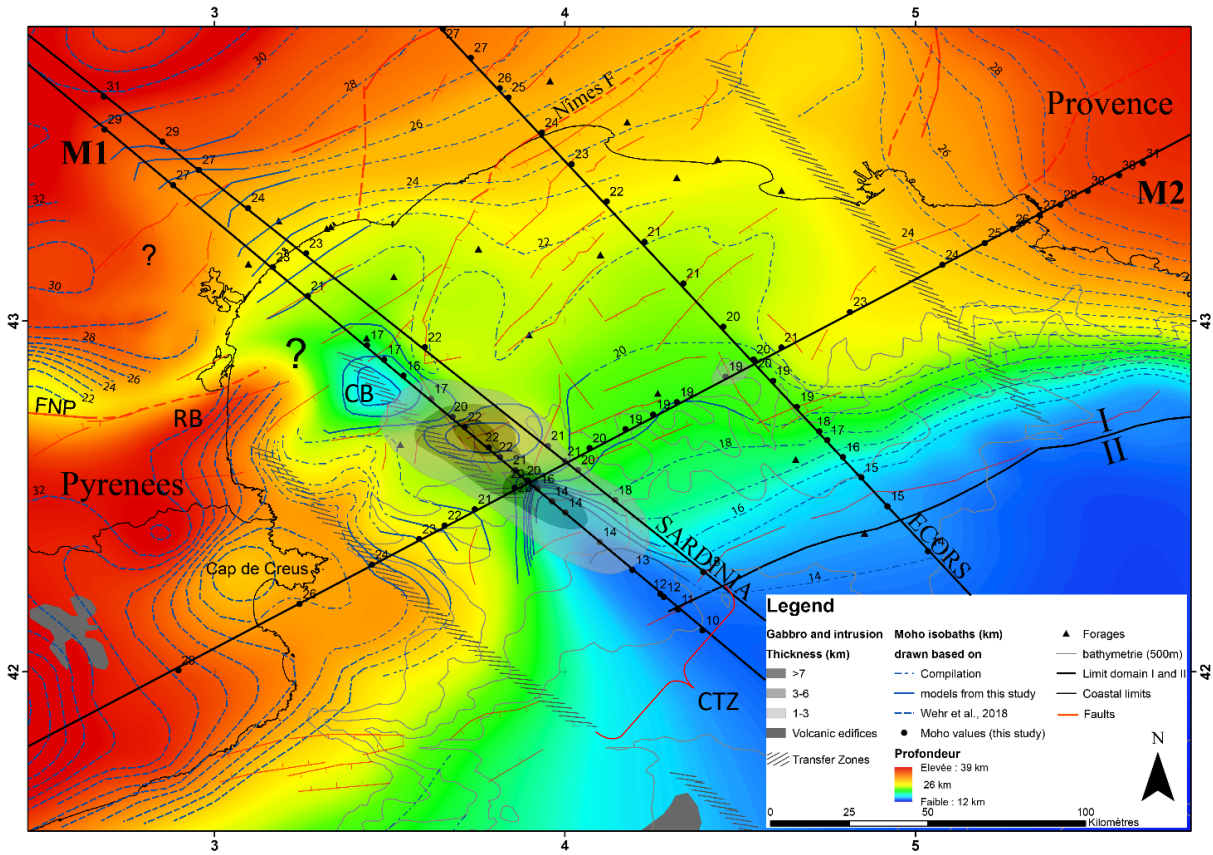


Figure 8

a)



b)

